International Journal of Coal Geology xxx (xxxx) xxx

Contents lists available at ScienceDirect

International Journal of Coal Geology

journal homepage: www.elsevier.com/locate/coal

Comprehensive evaluation of potential coal mine dust emissions in an open-pit coal mine in Northwest China

Pedro Trechera [a,b,*], Teresa Moreno [a], Patricia Córdoba [a], Natalia Moreno [a], Xinguo Zhuang [c], Baoqing Li [c], Jing Li [c], Yunfei Shangguan [c], Ana Oliete Dominguez [d], Frank Kelly [d], Xavier Querol [a,c]

[a] Institute of Environmental Assessment and Water Research (IDAEA-CSIC), 08034 Barcelona, Spain
[b] Department of Natural Resources and Environment, Industrial and TIC Engineering (EMIT-UPC), 08242 Manresa, Spain
[c] Key Laboratory of Tectonics and Petroleum Resources, China University of Geosciences, Ministry of Education, Wuhan 430074, China
[d] MRC-PHE Centre for Environment and Health, King's College London, London SE1 9NH, UK

ARTICLE INFO

Keywords:
Coal mine dust
Oxidative potential
Tailings
Mineralogy
Particle size
Geochemistry
Respirable dust fraction

ABSTRACT

Coal mining in China is continually increasing, and the associated emitted coal mine dust is of growing environmental and occupational concern. In this study, deposited coal mine dust (DD) was analysed in three different regions of an active, highly-volatile bituminous open-pit coal mine in the Xingjian Province, Northwest of China: coal working fronts, tailings handling sites, and road traffic sites. Samples were analysed for particle size, and geochemical and mineralogical patterns, and then compared with the respirable DD fractions (RDDs, <4 μm) separated from DD samples. Online measurements of ambient air concentrations of particulate matter (PM_{10} and $PM_{2.5}$), black carbon (BC) and ultrafine particles (UFP) were performed in the same mine zones where DD was sampled.

Furthermore, the RDD samples were subjected to analysis of specific biological response or toxicological indicators (oxidative potential, OP). The results demonstrated: i) large differences in particle size and composition among DD from tailings handling, road traffic and coal working front sites, ii) a strong influence of the DD moisture contents and ash yields on particle size, and, accordingly, on the potential dust emissions, iii) an enrichment of multiple elements (such as Nb, Th, Cr, Sr, Li, As, Pb, Cu, Zr and Ni) in the RDD from coal working fronts compared with their contents in the worked parent coal seams, mostly attributed to mining machinery, tyre and brake wear emissions and to deposition of dust emitted from gangue working zones, iv) low OP values of the RDD emitted from the studied mine, which works a high-quality coal, with OP being influenced by Mn, sulphate and anatase (TiO_2) contents, and v) the impact of specific mining operations and mine areas on the levels of air pollutants, such as high PM from tailings handling in the upper parts of the mine or the high UFP levels in the bottom of the mine (due to vehicle and machinery emissions and lower dispersive conditions). The data presented here demonstrate the necessity of extracting the more deeply respirable size fraction of coal mine dusts in future studies on the health effects of these materials because this finer fraction is mineralogically and geochemically different from the parent rocks.

1. Introduction

Coal represents the second most consumed energy source worldwide, accounting for 27.2% of the total, less only than oil (33.6%) (BP, 2019). Even though consumption of coal is decreasing in some regions, such as Europe and North America, coal consumption will continue to increase during the next two decades according to the International Energy Agency (IEA), World Coal Association (WCA) and British Petroleum (BP) (BP, 2019; IEA, 2019; WCA, 2020). The Asiatic Pacific region will be principally responsible for this increase, as increased demand and extraction of coal are expected there in the near future. The primary demand originates mainly from China, where coal is the main energy source (58.2% of total energies consumed). This makes it the principal country consumer of coal (50.5%), followed by India and USA (12.0%

* Corresponding author at: Institute of Environmental Assessment and Water Research (IDAEA-CSIC), 08034 Barcelona, Spain.
E-mail address: pedro.trechera@idaea.csic.es (P. Trechera).

https://doi.org/10.1016/j.coal.2021.103677
Received 29 July 2020; Received in revised form 23 December 2020; Accepted 1 January 2021
Available online 8 January 2021
0166-5162/Crown Copyright © 2021 Published by Elsevier B.V. This is an open access article under the CC BY-NC-ND license (http://creativecommons.org/licenses/by-nc-nd/4.0/).

and 8.4%, respectively)(BP, 2019).

Coal can be extracted by two mining methods, surface mining and underground mining, both depending on topographical features, accessibility, overburden thickness, and groundwater presence, among other factors (Lee, 1990). In open-pit coal mining, dust produced during coal extraction is a ubiquitous health concern, but other related processes can also produce dust. So, in open-pit coal mines, multiple activities must be taken into account when analysing the environmental conditions in the different sections to ensure safety for the workers and other individuals surrounding the mine. These activities include: i) drilling and extraction of rocks and sand necessary to find the coal seam, ii) explosion control to remove rocks in the area of interest, iii) coal mine dust gangue manipulation, extraction and transportation, iv) use of different diesel and gasoline transportation machinery (trucks, drillers, washers, excavators, and others), and v) coal extraction and transportation.

Coal mine dust is a common hazard generated during coal production. This is a complex and heterogeneous mixture composed of particles of different sizes and compositions from a variety of minerals, organic compounds and coal species (Caballero-Gallardo and Olivero-Verbel, 2016; Dalal et al., 1995; Liu et al., 2005; Pedroso-Fidelis et al., 2020). All these characteristics depend on the properties of the parent coal and gangue, and the different mining activities conducted in the coal mines (Dalal et al., 1995). It is important to consider the suspended respirable fraction (particle size <4 μm) of coal mine dust produced during coal activities, since it is primarily responsible for coal workers' pneumoconiosis (CWP) and silicosis (Cheng et al., 2016; Erol et al., 2013; Shi et al., 2019). Moreover, high levels of coal mine dust can present a significant risk of spontaneous combustion in (mostly underground) coal mines (Liu et al., 2010; Ma et al., 2020; Shimura and Matsuo, 2019). Furthermore, coal and coal gangue fires might occur in open-pits, which would result in the emission of both particulate and gaseous pollutants.

Due to technical improvements, finer coal milling products, and increased efficiencies for coal extraction are occurring in coal mines, and accordingly coal mine (finer) dust emissions have increased. Simultaneously, CWP injuries have also risen (Gamble, 2012; Johann-Essex et al., 2017; Sarver et al., 2019; Suarthana et al., 2011), influenced by these and possibly other factors such as the size of the mine, the miners' tasks and type of coal could also affect the increase in CWP (Sarver et al., 2019; Suarthana et al., 2011).

One of the major concerns regarding occupational health relevance is the particle size of suspended coal mine dust, sensu *lato,* which originates from the above multiple mining activities and emission sources (Richardson et al., 2018), including also soot from vehicles and machinery or coal self-combustion.

Coal mine dust is generally coarse in size, with its suspended mass being coarser than the respirable particulate matter (PM) fraction PM_4 (<4 μm). Thus, studies carried out along coal conveys into mines have measured low (4–13%) contents of respirable dust in ambient bulk coal dust, defined as coal dust particles with a diameter ≤ 74 μm (Shahan et al., 2017). On the other hand, atmospheric PM emissions from exhaust and spontaneous coal burns would be expected to have a dominantly ultrafine particle (UFP) size (< 0.1 μm) (Dias et al., 2014; Kurth et al., 2014). These two types of ambient suspended particles (PM_4 and UFP) likely have different occupational health effects. The former are retained in the alveoli and thus may damage mainly the respiratory systems (WHO, 2013), whereas the latter are potentially capable of passing through the lung to enter the circulatory system, to be translocated to other organs of the body (Cassee et al., 2019, 2011; Heusinkveld et al., 2016).

The presence of respirable crystalline silica (RCS) in coal mine dust is extremely important as this is known to be responsible for CWP injuries and lung cancer (Brodny and Tutak, 2018; Castranova, 2000; Cohen et al., 2008; NIOSH, 2002). Furthermore, the elevated content of metals and/or some organic pollutants in the dust could substantially increase the oxidative stress caused by mining dust, thus also increasing potential precursors of some injuries (Birben et al., 2012; Ghio and Madden, 2018; Ercal et al., 2005; Schins and Borm, 1999; Valko et al., 2016). Some metals and metalloids (Fe, Ti, Mn, Cu, Sb, Sn, Pb, Zn, Cr, V, As and Ni) present in the respirable fraction in high concentrations can produce negative health effects in humans (Dai et al., 2014; Dai and Finkelman, 2018; Finkelman, 1994; Fu et al., 2014; Hower and Robertson, 2003; Latvala et al., 2016; Moreno et al., 2019; Riley et al., 2012).

The aim of the present work is to evaluate the potential dust emissions in an open-pit coal mine working high-quality Jurassic coal in the Xinjiang Province, Northwest of China. To this end, a detailed study of the open-pit mine was carried out, where mining dust generated different activities and sources were measured, sampled and analysed. The analyses include particle size, morphology, chemistry, mineralogy and oxidative stress of deposited dust (DD) and the respirable DD fraction (RDD) separated from the DD which was collected in multiple dust hotspots in the mine. The parent coal was analysed for comparison purposes with the DD and RDD from the working front. Furthermore, online exposure measurements for PM finer than 2.5 and 10 μm ($PM_{2.5}$ and PM_{10}), black carbon (BC), and UFP, were also included for comparison of the impact of different mining activities on exposure to these pollutants.

2. Geological setting

Wucaiwan open-pit coal mine is located in Jimusaer County, Xinjiang Province, Northwest of China (Fig. 1A). The open-pit covers approximately 24 km^2 and contains recoverable coal reserves of approximately 1.7 billion tones. The annual production capacity of coal mine is 20 million tonnes in 2017. This coal mine was opened since 2006, with an estimation of 63 years of life.

The Wucaiwan open-pit coal mine is located in the Western margin of Eastern Junggar Coalfield (Fig. 1B), where the Jurassic Badaowan, Sangonghe, and Xishanyao Formations are the coal-bearing strata (Fig. 1C). Among these, the Middle Jurassic Xishanyao Formation is the predominant coal-bearing unit, and, it is made up by finely grained sandstone, with coal seams, and minor siltstone and carbonaceous mudstone (Fig. 1D). The Xishanyao Formation conformably overlies the Early Jurassic Sangonghe Formation and conformably underlies the Late Jurassic Shishugou Formation (Fig. 1D). Based on the coal exploration data of Eastern Junggar Coalfield, the thickness of the Xishanyao Formation in the Wucaiwan open-pit coal mine ranges from 37 m to 198 m with an average of 136 m; it contains one workable coal seams, and, its average thickness is 60 m.

Previous coal exploration data of Eastern Junggar Coalfield show that the Middle Jurassic mineable coal seam is high-volatile bituminous and contains medium moisture content (≈13%), low ash yield (≈6%), and low sulphur content (≈0.4%). The coal quality is discussed in detail in previously published papers (Li et al., 2012; Zhou et al., 2010).

3. Methodology

3.1. Sampling

A total of seven tailing and coal working zones were examined in the Wucaiwan open-pit coal mine over two working days. These sample locations were selected to characterise dust from most mining activities in the open-pit. These included coal extraction (coal front), coal transportation, drilling, truck traffic and tailings handling. Fig. 1C shows a simplified map of the open-pit mine and the investigated zones. Dust from coal working front was studied in the C and D zones, where, in addition, two-parent coal channel profiles (CPs) were sampled.

Table S1 summarises the location and origin of the thirteen DD samples collected (six in coal fronts and seven in tailing-related activities). DD samples were collected using plastic trays and brushes, and, kept in sealed plastic bags until analysis. Trays were left in the vicinity of the specific operations for approximately thirty minutes, until DD mass

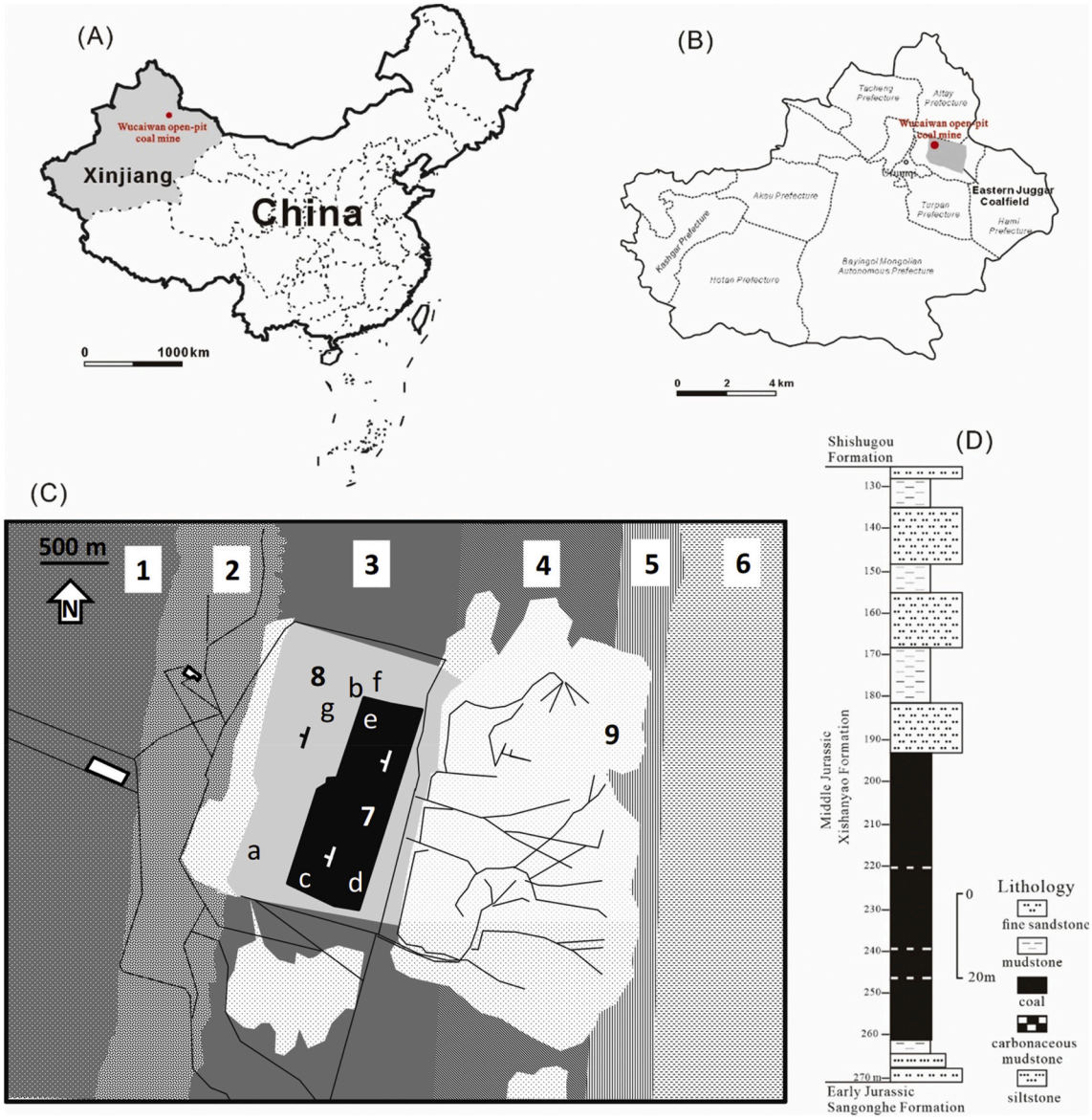

Fig. 1. Location of Wucaiwan open-pit coal mine in China (A), and, in Xinjiang Province, Northwest of China (B). Geological map of the Wucaiwan open-pit coal mine with the working areas where measurements of meteorological parameters, BC, UFP, PM_{10}, $PM_{2.5}$ and sampling of PM, deposited dust and coal channel profiles were carried out (C). Stratigraphic series of Wucaiwan open-pit (D). *a/b-TH, Tailings handling; c/d/e- CWF, Coal working front; f-TH; g-RT, Road traffic into a mine road for tailings. Legend: 1-Quaternary; 2-Middle-Late Jurassic Shishugou group; 3-Middle Jurassic Xishanyao formation; 4-Early Jurassic Sangonghe formation; 5-Early Jurassic Badaowan formation; 6-Middle-Late Triassic Xiaoquangou group; 7-Worked coal outcrops; 8-Tailings disposal into the pit; 9-Tailings disposal outside the pit.*

(around 200–500 g) was enough for subsequent analysis. Samples were stored without light, hermetically closed and at room temperature to prevent oxidation processes. Passive stubs for scanning electron microscopy with energy dispersion spectroscopy (SEM-EDS) analyses with graphite label surfaces were placed in all zones for 1-h collection of ambient air samples. Finally, real-time measurements of ambient concentrations of suspended PM, BC and UFP, as well as meteorological parameters, and sampling of PM_{10} were carried out at the above seven locations where DD was sampled, Tables S2 and S3.

Ambient air PM_{10}, PM_4, or $PM_{2.5}$ were generally not sampled because the sampling work was allowed inside the mine for only one day and a half. Given this time constraint, collecting DD and extracting from it RDD (at the laboratory) allowed the sampling of different areas and operations. Thus, a limitation of the study is that RDD was not air sampled but obtained from DD. This study does not take into account how, for example, the intensity of different mining activities might change over time, or how varying meteorological conditions might affect dust loading. However, sampling in numerous locations provided very valuable information. In any case this is an arid region and relative humidity (RH) is normally low and similar to that one measured during sampling campaign. Finally, one clear advantage was that the whole sampling campaign was carried out while the coal mine workers were performing their daily work operations with total normality, thus allowing us to capture a representative snapshot of a typically working day in the open-pit mine.

3.2. Analysis

3.2.1. Sample pre-treatment and particle size

Before analysis, all DD samples collected were sieved <500 μm (with only a very minor amount being >500 μm). After this point DD will be refer to this <500 μm DD fraction. Then, DD samples were riffled to obtain two sub-samples of 100 g, from one of which 50 g were used for RDD extraction. Sub-samples of 0.10 to 2.0 g were obtained from the DD

and RDD for the different analyses. A total of thirteen DD (Table S1) and two CP samples were collected from open-pit coal mine areas where most dust emitting mining activities were conducted, and these were compared with the parent coal. A mechanical dust size-separator device (Moreno et al., 2005) was used in the laboratory to separate the RDD from the DD samples. Since obtaining RDD from DD is a laborious task, eight from the thirteen DD samples were selected to this end, based on the similarity of particle size distribution (PSD), mineral and chemical compositions and covering all the locations sampled. Thus, four DD samples were selected from the coal working and four from tailings handling. Around 50 g of untreated DD samples were introduced into the PM separator to be mechanically re-suspended in a rotator and a pump at 25 L·min^{-1} to separate the RDD fraction on polycarbonate filters (47 mm diameter, 0.60 μm pore size). The size distribution of each collected RDD was measured to confirm their respirable size (<4 μm).

A Malvern Mastersizer was used for PSD analysis of DD and RDD samples, 1.0 g and 0.25 g respectively. A Scirocco 2000 extension was used to analyse the particle size in dry conditions when a large sample volume was available, and a HydroG 2000 extension was used for low sample volumes, following the method of Sperazza et al. (2004) based on suspension in a Na polyphosphate solution. Malvern Mastersizer Scirocco 2000 extension measurements were performed at the ICTS NANBIOSIS by the Nanostructured Liquids Unit (U12) of the CIBER in Bioengineering, Biomaterials & Nanomedicine (CIBER-BBN), located at the IQAC-CSIC (Barcelona, Spain).

3.2.2. Mineralogical and morphological characterisation

Mineralogical characterisation of 1.0 g of CP and DD, and 0.30 g of RDD samples were conducted by powder X-ray diffraction (XRD). A Bruker D8 Advance A25, θ-θ diffractometer with CuKα1 radiation, Bragg-Brentano geometry, and a position-sensitive Lynx Eye detector, was used for these analyses. Diffractograms at 40 kV and 40 mA, scanning from 4 to 60° of 2 θ with a step size of 0.019° and a counting time of 0.10 s·step^{-1} maintaining the sample in rotation (15 min^{-1}) were performed. The crystalline phase identification was conducted using the EVA software package (Bruker), which utilised the ICDD (International Centre for Diffraction Data) database. Semi-quantitative XRD analysis was performed using the method devised by Chung (1974) for the quantitative analysis of multi-component systems, using quartz as an internal reference. Mixtures were obtained using powdered mineral reference materials and coal with very low ash to validate the semi-quantitative protocol (Fig. S1).

Scanning electron microscope JEOL JSM-7001F SEM-EDX with secondary and backscattered electron detectors from the Scientific-Technical Services of the University of Barcelona was used for morphological and chemical analysis of single particles deposited on the graphite surface of the passive samplers. To this end gold coating was used to qualitatively analyse the occurrence of specific RDD components of interest according the correlation of oxidative potential (OP) and mineral and elemental compositions.

3.2.3. Proximate, ultimate and chemical characterisation

Proximate and ultimate analyses followed ISO and ASTM procedures (ISO-589, 1981, ISO-1171, 1976, ISO-562, 1974, ASTM D-3286, D-3302M, D3174-12), with moisture and ash yields obtained at 150 °C and 750 °C, respectively. The amount of sample used was always around 0.50 g.

Before geochemical analysis, 0.10 g of samples were digested in HF-HNO_3-$HClO_4$ acid following the method by Querol et al. (1997, 1992) to retain potentially volatile elements, such as As and Se. The resulting acidic digestions were analysed for major and trace elements by using inductively-coupled plasma atomic-emission spectrometry (ICP-AES, Iris Advantage Radial ER/S device from Thermo Jarrell-Ash) and inductively-coupled plasma mass spectrometry (ICP-MS, X-SERIES II Thermo Fisher Scientific, Bremen, Germany). International reference materials SARM19 and NIST SRM 1633b, and blanks were treated in the same way. Because Si is lost during HF digestion, its content in DD and RDD samples was determined by X-ray fluorescence (XRF, Thermo Scientific ARL QUANT'X Energy-Dispersive X-ray fluorescence spectrometer) loading Teflon© 47 mm filters with 3.0 mg of the sample using an ethanol suspension. XRF Si/Al ratios obtained were applied to the Al determined by ICP-AES analysis of each sample. This method was validated using the above reference materials.

After five repetitions of the analysis of the above reference materials, analytical errors were estimated at ±1–6% for most major elements in both the SARM19 coal and NIST-1633b fly ash reference materials, with the exceptions of P in SARM19 (16%) and Na in the latter (10%, with relative standard deviations [RSDVs] ranging from 1 to 8%, with P exception in NIST-1633b-fly ash, 10%). Most of trace element errors for all certified and 'for reference' elements in SARM19 coal were in the range of ±0–5%, with the exception of Li, Sc, Ni, Cu, Zn, Y, Sn, Gd, Pb (±6–10%); Be, Se, Lu, Hf, W (±11–20%); Zr (27%), Cd (29%), Tm (31%), Sb (80%) and ± 0–5% for all certified and 'for reference' elements in NIST-1633b-fly ash, with the exception of Sc, Cu, Zn, Ge, Nb, Sn, Eu (6–10%); Be, Mo, Cd, Gd, Lu, Hf, Bi (11–20%); and Zr (21%), Tm (28%), Ta (30%) with RSDV <10% for most elements, with the exception of Y(11%), W (14%), Gd (15%), Sn (18%), Hf (18%), Li (20%), Tb (22%), Sb (23%), Zr (29%), Cd (46%), Zn (50%), Ta (52%) and Se (60%) for SARM19 and < 10% for all elements, with the exception of Lu (13%), Gd, Tm, Ta (29%) for NIST-1633b.

3.3. PM_{10} measurements

Ambient air PM_{10} in the mine was measured and collected using personal environmental monitoring (PEM) samplers equipped with Leland Pumps (10 L·min^{-1}) on PAL high purity 37 mm quartz microfibre filters of 2.0 μm pore size. Table S2 provides the location and duration of the four PEM samplings. Filters were weighed before and after sampling previous equilibrium over 48 h at 50% RH and 20 °C.

The PM_{10} filters were acid (HF-HNO_3-$HClO_4$) digested following the method by Querol et al. (2001). The resulting acidic digestions were analysed for major and trace elements using the above ICP-AES and ICP-MS instrumentation. These quartz filters have very low contents of major and trace elements and are widely used in air quality studies, but in any case, blank digestions and analyses were carried out and the blank concentrations for each element analysed subtracted of each sample.

3.4. Online measurements

To measure real-time ambient concentrations of suspended PM in emission hotspots in the open-pit, three real-time monitors were used in seven locations from zones A to G (Fig. 1C). For $PM_{2.5}$ and PM_{10} mass concentrations (in μg·m^{-3}), a Dust-track-TSI and an AirVisual Pro were used in all the zones of the mine, with a 30 s resolution. The latter also measured temperature (°C), RH (%) and CO_2 concentrations (ppm). For BC (μg·m^{-3}) and UFPs number concentration (#cm^{-3}), mainly influenced by the exhaust emissions of on-road and off-road vehicles/machinery, a microAeth® AE51 (zones A, C, D) and DiSCmini (zones A, C, D) monitors were used with a 10 and 60 s resolution. Table S3 summarises the relevant details of these measurements. Prior to use, instruments were compared with reference instruments: a GRIMM 1108 optical counter for Airvisual Pro (IQAir) and Dust-track, a CPC-TSI for Disc-mini, and a MAAP-Thermo for microAeth® AE51 (Fig. S2). Online measurements were always carried out close to the DD sample collection point of each zone, with the procedure in each case being: i) switching online measurements and PM sampling, ii) collecting DD samples, and iii) finishing online measurements and PM sampling.

3.5. Oxidative potential test

Oxidative potential was determined using a synthetic respiratory tract lining fluid (RTLF) validated by Mudway et al. (2004) and Zielinski

et al. (1999) containing the toxicological indicators, such as ascorbate (AA), urate (UA) and reduced glutathione (GSH) found in the surface of the lung. This is widely used to characterise the OP of atmospheric particles (Kelly, 2003, and references therein). When the particles are added to a solution of these tracers, the oxidation of AA, UA and GSH might occur as a function of their composition and size.

The oxidative stress of the RDD samples was evaluated by measuring the OP based on the consumption of the antioxidants AA, UA and GSH, according to the methodology by Soltani et al. (2018). This technique involves the resuspension of mg of each RDD in ethanol followed by a 4 h incubation with a synthetic solution containing equimolar concentrations of AA, UA and GSH. The consumption of AA, UA and GSH was determined by previously published methodology (Baker et al., 1990; Iriyama et al., 1984). In-house controls of PM-free, negative (M120, Cabot Corporation, USA) and positive PM (NIST1648a, urban particulate from NIST, USA) followed the same protocol for control purposes. The OP is expressed as the percentage of consumption of each antioxidant with reference to the in-house particle-free control. To obtain a metric for OP, the data was expressed as $OP{\cdot}\mu g^{-1}$ of PM ($OP^{AA}{\cdot}\mu g^{-1}$ PM and $OP^{GSH}{\cdot}\mu g^{-1}$ PM). Data for the individual antioxidants were also combined to provide a total OP value ($OP^{TOTAL}{\cdot}\mu g^{-1}$).

4. Results

Sampling and measurements focused on three major activities: coal working fronts, tailings handling, and road traffic in the open-pit. Major patterns of DD samples and variability of ambient air levels of the studied pollutants in relation to these zones are described, with the intention of characterising dust from different activities and sources and identifying potential dust hazards for each activity. The section on results is divided into two parts, the first dealing with DD, RDD and OP, and a second on atmospheric measurements.

4.1. Deposited dust and respirable deposited dust

4.1.1. Particle size

Table 1 shows the analysed PSD patterns of DD samples using the dry method, as well as the respective moisture contents and ash yields. Fig. 2 compares data from the three mining activities listed above.

At the coal working fronts, DD was markedly coarser than at both tailings handling and road traffic sites, where DD had higher ash yields and lower moisture contents. The coal working fronts DD fractions <500 (DD500), <10 (DD10), <4 (DD4), and < 2.5 μm (DD2.5) reached 19–32, 9–15 and 5–9%volume (%vol), respectively, which were considerably lower than those of tailings handling (18–55, 11–38 and 6–27%vol), and road traffic (36, 23 and 15%vol), respectively. The moisture content of DD has been reported as a major driver of resuspension (Amato et al., 2010; Colinet et al., 2010; Medeiros et al., 2012; Xi et al., 2014). Eqs. (1) to (4) and fig. S3 (1–4) show the cross-correlation, using Pearson's correlation coefficients (r), of moisture contents with the proportion of the <500, <10, <4, and < 2.5 μm fractions of DD samples from the coal working fronts.

4.1.1.1. Coal working front

$$DD500\ (\%vol < 500\ \mu m) = -1.84*Moisture\ (\%ad) + 107.18\ (r = -0.60) \quad (1)$$

$$DD10\ (\%vol < 10\ \mu m) = -0.77*Moisture\ (\%ad) + 32.98\ (r = -0.66) \quad (2)$$

$$DD4\ (\%vol < 4\ \mu m) = -0.37*Moisture\ (\%ad) + 15.92\ (r = -0.71) \quad (3)$$

$$DD2.5\ (\%vol < 2.5\ \mu m) = -0.43*Moisture\ (\%ad) + 10.71\ (r = -0.92) \quad (4)$$

The results indicate a clear (r = −0.92) decrease of the DD2.5 fraction with increasing moisture. In the case of the coarser fractions, the negative correlation persists but with lower significance (r = −0.60 to −0.71). This indicates that lower DD2.5 was available for resuspension in moistened DD. As it might be expected, high moisture in DD reduces the occurrence of DD2.5 due to the agglomeration effect caused by water. Sprayed water is frequently applied to the coal working fronts and unpaved mine roads to reduce re-suspension (Zhang et al., 2012). As shown in Table 1, coal working front DD samples reached the highest moisture contents due to the greater coal content in DD, but also because of the frequent wetting of the coal mine dust surfaces.

No correlation was found between DD and moisture in the tailings handling zone, probably because water is not spread in these areas of tailings disposal and moisture contents are very low. In this area some samples, usually located at the high-altitude zones of the pit, the RDD reached very high proportions of 20–38%vol of DD (samples BNW_DD_001, 008 and 009), much higher than in the wetter and coaly DD from the working front. This dry tailing DD has accordingly an increased resuspension potential during windy episodes and during transport of tailings, compared to DD from the coal fronts.

Eqs. (5)–(8) and fig. S3 (5–8) show the same regressions as above, but in this case, between the ash yields (% dry basis, db) from the coal working fronts. A clear positive correlation can be observed, (even higher than those for moisture contents), especially for DD2.5 ($r = 0.99$, excluding BNW_DD_013) with the ash yields (%db). Coals containing an elevated mineral content, usually fine clays and quartz, yield to a greater proportion of DD2.5 in DD than more low-ash yield varieties, the organic matrix of which produces coarser grains when breaking up into particles (Rosita et al., 2020; Sevim and Demir, 2019; Yang et al., 2019).

4.1.1.2. Coal working front

$$DD500\ (\%vol < 500\ \mu m) = 1.13*Ash\ yield\ (\%db) + 74.36\ (r = 0.67) \quad (5)$$

Table 1
Particle size distribution and results of proximate analysis of deposited dust (DD, <500 μm) samples. *TH, Tailings handling; CWF, Coal working front; RT, Road traffic into a mine road for tailings. M, moisture, HTA, Ash yield.*

Sample	Location	<500 μm (%wt)	<10 μm (%v)	<4 μm (%v)	<2.5 μm (%v)	M (%ad)	HTA (%db)
BNW_DD_002	C –CWF	99.03	30.25	14.02	8.70	5.50	24.78
BNW_DD_012	C –CWF	99.53	25.27	11.86	7.25	5.52	16.50
BNW_DD_005	C –CWF	63.89	18.63	12.80	4.86	12.47	5.84
BNW_DD_006	D –CWF	86.98	20.92	9.39	4.58	13.62	7.53
BNW_DD_013	D –CWF	94.20	31.57	15.16	8.73	7.40	7.22
BNW_DD_007	E –CWF	89.71	25.01	9.91	4.61	15.20	4.75
BNW_DD_001	A –TH	97.65	55.25	38.02	26.53	0.80	90.49
BNW_DD_010	B –TH	96.47	28.30	18.64	12.87	0.57	90.03
BNW_DD_011	B –TH	91.38	18.39	10.47	5.63	2.51	94.05
BNW_DD_003	B –TH	80.17	18.45	11.35	5.61	2.44	93.11
BNW_DD_004	B –TH	92.13	23.70	13.89	8.31	2.25	93.08
BNW_DD_008	F–TH	94.54	32.22	20.84	13.41	3.70	90.95
BNW_DD_009	G–RT	96.45	36.12	23.29	15.20	2.17	92.82

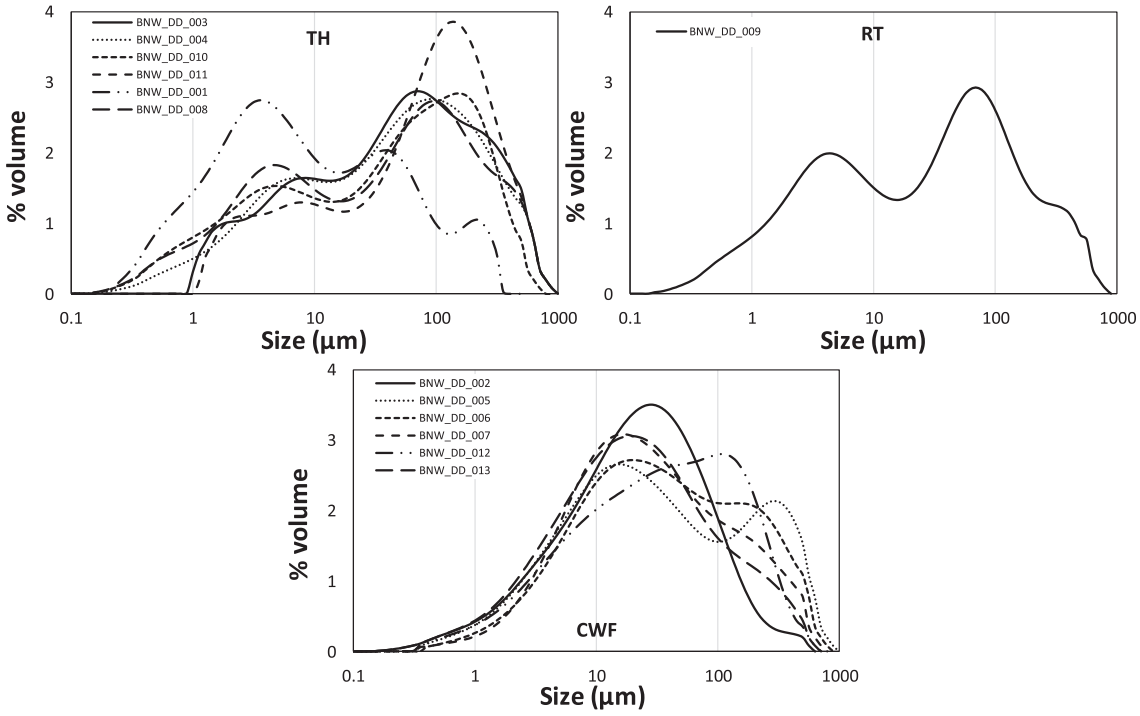

Fig. 2. Particle size distribution of deposited dust (DD, <500 µm) samples from the open-pit coal mine split by the three type of activities. *TH, Tailings handling; CWF, Coal working front; RT, Road traffic into a mine road for tailings.*

$$DD10\ (\%vol < 10\ \mu m) = 0.43*\text{Ash yield}\ (\%db) + 18.96\ (r = 0.82) \quad (6)$$

$$DD4\ (\%vol < 4\ \mu m) = 0.16*\text{Ash yield}\ (\%db) + 9.70\ (r = 0.70) \quad (7)$$

$$DD2.5\ (\%vol < 2.5\ \mu m) = 0.22*\text{Ash yield}\ (\%db) + 3.43\ (r = 0.99) \quad (8)$$

In contrast, the very high ash yields of DD from tailings handling (Eqs. (9)–(12) and fig. S3, 9–12) are negatively correlated with the proportions of DD10, DD4 and DD2.5 ($r = -0.86$ to -0.94, excluding BNW_DD_001). Because all DD samples from tailings handling had very low coal content (< 5%), the changes in the proportions of the fine fraction in DD due to elevated coal contents (low ash yield) cannot be evaluated. However, the fine fraction of DD increases as carbonate minerals decrease, and clay and quartz increase.

4.1.1.3. Tailings handling

$$DD500\ (\%vol < 500\ \mu m) = -2.17*\text{Ash yield}\ (\%db) + 290.68\ (r = -0.57) \quad (9)$$

$$DD10\ (\%vol < 10\ \mu m) = -3.13*\text{Ash yield}\ (\%db) + 312.87\ (r = -0.86) \quad (10)$$

Table 2
Mineral contents in deposited dust (DD, <500 µm) and channel profile (CP) samples. Values in %wt. Gypsum (Gp), Qtz (Quartz), Anatase (Ant), Calcite (Cal), Microcline (Mc), Albite/Anorthite (Ab/An), Illite/Muscovite (Ilt/Ms), Kaolinite/Clinochlore (Kln/Clc). *TH, Tailings handling; CWF, Coal working front; RT, Road traffic into a mine road for tailings.*

Sample	Zone	Ilt/Ms	Kln/Clc	Qtz	Ab/An	Mc	Cal	Gp	Ant	Total
BNW_DD_002_CWF	C	0	8.9	15	0	0	0	0.5	0	25
BNW_DD_012_CWF	C	0	6.3	8.4	1.1	0	0	0.7	0	17
BNW_DD_005_CWF	C	0	3	2.2	0	0	0	0.6	0	5.8
BNW_DD_006_CWF	D	0	3.1	1.4	0	0	0	3.1	0	7.5
BNW_DD_013_CWF	D	0	1.8	4.1	0	0	0	1.3	0	7.2
BNW_DD_007_CWF	E	0	0	1.1	0	0	0	3.7	0.3	5.1
BNW_DD_001_TH	A	8.6	56	33	0.3	0	0.8	0.4	0.6	100
BNW_DD_010_TH	B	1.4	8.1	40	16	0.6	34	0	0.5	100
BNW_DD_011_TH	B	2.2	9.6	78	8	1.2	0	0	0.9	100
BNW_DD_003_TH	B	2.8	19	61	8	1.5	7	0	1.1	100
BNW_DD_004_TH	B	5.6	25	60	3.8	1.4	3.7	0	0.7	100
BNW_DD_008_TH	F	2.1	29	64	2.5	0.9	0	0.3	0.7	100
BNW_DD_009_RT	G	1.9	12	71	12	1.2	0	1	0.8	100
BNW_CP_001	C	0	2.6	1	0	0	0	0	0	3.6
BNW_CP_002	D	0	3.2	0	0	0	0	0	0	3.2
BNW_RDD_002_CWF	C	0	12	12	0	0	0	0.2	0	25
BNW_RDD_005_CWF	C	0	3.8	1.7	0	0	0	0.4	0	5.8
BNW_RDD_006_CWF	D	0	4.5	0.4	0	0	0	2.7	0	7.5
BNW_RDD_007_CWF	E	0	0	1.8	0	0	0	3.0	0.3	5.1
BNW_RDD_001_TH	A	9.7	74	15	0.3	0	0.6	0.3	0.3	100
BNW_RDD_003_TH	B	3.5	25	56	1.6	0.9	12	0	1.1	100
BNW_RDD_008_TH	F	2.5	30	64	0.9	1.5	0	0.8	0.6	100
BNW_RDD_009_RT	G	2.4	13	82	1.2	0.6	0	0.6	0.3	100

$$DD4\ (\%vol < 4\ \mu m) = -2.47*\text{Ash yield}\ (\%db) + 242.93\ (r = -0.91) \quad (11)$$

$$DD2.5\ (\%vol < 2.5\ \mu m) = -2.12*\text{Ash yield}\ (\%db) + 204.41\ (r = -0.94) \quad (12)$$

4.1.2. Mineralogy

The worked coal is a high quality one, with very low yields, due to low content of kaolinite (3%weight, %wt) and quartz (1%wt) identified by XRD (Table 2), and low S contents (Tables 3 and S4 and fig. S4, a–b). As expected, the mineral contents of coal working front DD samples increased (up to 9%wt kaolinite/clinochlore, 1–15%wt quartz, and with up to 3.7%wt gypsum, and traces, < 1.0%wt, of albite/anorthite, and anatase) compared to the parent coal. All coal working front DD samples were collected close to the main 72 m-thick very low-ash coal seam. Thus, the elevated mineral content of the DD compared with the parent coal is attributed to dust deposition from the tailings handling operations, the occurrence of partings in the coal seam (not sampled in the channel sampling profile of this work), the emissions of dust deposited on trucks, drilling and mine explosions, and the contributions of external windblown dust.

Also as expected, the mineral composition of DD samples from tailings handling and road traffic is entirely different from the one from the coal working fronts, showing greater clay and quartz contents, with illite/muscovite being the major minerals (10–65 and 14%wt clays and 34–78 and 71%wt quartz, respectively, Table 2). Furthermore, calcite content in some of the tailings handling DD samples reached up to 34% wt, and feldspars and anatase 0.3–16 and 0.5–1.1%wt respectively, in both tailings handling and road traffic DD (Table 2). Conversely, gypsum contents decreased with respect to DD from the coal working front. The slight increase in gypsum content in the latter is suggested to be due to the excess of humidity resulting from the spreading of water containing dissolved sulphate, favouring the oxidation of sulphides from DD. The occurrence of trace amounts of pyrite in coal and the high humidity might cause the oxidation of this mineral and the generation of gypsum (Akinwekomi et al., 2020). In contrast, in the tailing and road truck zones, the lack of humidity, and probably the lower content of pyrite, might have reduced the formation of gypsum (Akinwekomi et al., 2020; Gomo, 2018; Madzivire et al., 2010). On the other hand, the reducing environments during peat deposition, combined with the effects of the interaction between dissolved Fe and H_2S cause enrichment of pyrite in coal, due to their bacterial reduction of sulphate ion (Casagrande, 1987; Dai et al., 2020; Querol et al., 1989) compared with more oxidising sedimentary environments, producing the pink to beige sediments converted into tailings. Road traffic and tailings handling DD samples had a very similar mineral composition because the road traffic site sampled is used for extraction of tailings.

4.1.3. Geochemistry

Major and trace element concentrations of DD and CPs are reported in Tables 3 and 4. The comparison of the concentrations of major and trace elements in the parent coal with the Chinese (Dai et al., 2008, 2007) and the worldwide (Ketris and Yudovich, 2009) averaged coal contents shows that the coal analysed in this study was depleted in most elements, with only Mg and Ba (1.1–1.5) and Sr and Na (1.6–2.0) having higher concentrations. The majority of the elements are enriched in the DD of the coal working front compared with the parent coal, an exception being in samples from zone B. The concentrations of most major and trace elements in the DD from tailings handling and road traffic were similarly higher than those from the coal working front. Mn is the only element with clearly different concentrations (488 $\mu g \cdot g^{-1}$ in tailings handling and 250 $\mu g \cdot g^{-1}$ in road traffic). Conversely, S, B and Sr were present in greater concentrations in the coal working front, and Ba in similarly elevated concentrations in all three types of DD.

Multiple potentially hazardous elements, such as Mn, Co, Ni, Zn, As and Cr (Finkelman, 1994), occurred in much larger concentrations in DD than in the parent coal, presumably due to dust deposition from the tailings handling zones, mining machinery and truck wear (Chen et al., 2015; Munir et al., 2020; Xu et al., 2017).

4.1.4. Respirable deposited dust

Table 5 shows the RDD particle size data (D50 and D90, median and percentile 90) separated from the DD by the PM separator. PSD analyses revealed that all RDD samples had a D50 in the range of 3–4 μm, which represent the respirable fraction. However, D90 values varied more widely depending on the type of DD. In the case of coal working front RDD, D90 reached 7–8 μm size but 4–5 μm in the tailings handling locations, making the RDD samples finer. As mentioned above, this might be due to the finer PSD of clay and quartz compared to the higher coarse coaly matrix proportion in the coal working front. In any case, the increased metal load and finer size patterns of the tailings handlings

Table 3
Major element contents in the deposited dust (DD, < 500 μm) and channel profile (CP) samples. Values in %wt. *TH, Tailings handling; CWF, Coal working front; RT, Road traffic into a mine road for tailings.*

Sample	Zone	Al	Si	Ca	Fe	K	Mg	Na	P	S
BNW_DD_002_CWF	C	2.32	5.23	1.08	0.52	0.31	0.27	0.59	0.01	0.44
BNW_DD_012_CWF	C	1.41	3.42	0.83	0.32	0.21	0.18	0.48	0.01	0.45
BNW_DD_005_CWF	C	0.27	0.53	0.73	0.08	0.04	0.29	0.37	<0.01	0.37
BNW_DD_006_CWF	D	0.19	0.29	1.21	0.07	0.03	0.21	0.83	<0.01	0.88
BNW_DD_013_CWF	D	0.37	0.79	0.77	0.09	0.04	0.33	0.56	<0.01	0.43
BNW_DD_007_CWF	E	0.19	0.3	0.71	0.09	0.01	0.13	0.48	<0.01	0.4
BNW_DD_001_TH	A	12.03	21.66	0.24	0.53	1.11	0.20	0.11	0.01	0.27
BNW_DD_010_TH	B	6.06	21.64	6.17	1.93	1.30	0.49	1.54	0.01	0.02
BNW_DD_011_TH	B	8.72	24.5	0.99	3.4	1.65	0.50	1.00	0.03	0.03
BNW_DD_003_TH	B	8.29	22.67	1.36	3.55	1.50	0.47	1.02	0.03	0.03
BNW_DD_004_TH	B	8.55	22.27	1.22	3.92	1.46	0.49	0.92	0.04	0.03
BNW_DD_008_TH	F	9.00	23.44	0.35	2.18	1.51	0.43	0.51	0.05	0.28
BNW_DD_009_RT	G	8.59	24.94	0.66	2.93	1.63	0.46	1.26	0.03	0.20
BNW_CP_001	C	0.10	0.20	0.79	0.05	0.02	0.17	0.23	<0.01	0.34
BNW_CP_002	D	0.07	0.11	0.63	0.06	0.01	0.18	0.25	<0.01	0.37
BNW_RDD_002_CWF	C	2.48	5.09	1.02	0.44	0.28	0.32	0.47	0.02	0.32
BNW_RDD_005_CWF	C	0.44	0.69	0.80	0.06	0.03	0.36	0.44	<0.01	0.35
BNW_RDD_006_CWF	D	0.40	0.47	1.82	0.03	0.04	0.27	0.89	0.01	1.32
BNW_RDD_007_CWF	E	0.21	0.22	0.67	0.10	0.01	0.17	0.57	0.01	0.32
BNW_RDD_001_TH	A	16.22	21.50	0.24	0.51	1.29	0.23	0.16	0.02	0.18
BNW_RDD_003_TH	B	9.80	28.71	2.18	4.62	1.59	0.60	0.77	0.05	0.16
BNW_RDD_008_TH	F	9.42	22.50	0.63	1.66	1.63	0.36	0.37	0.06	0.54
BNW_RDD_009_RT	G	9.71	22.77	0.67	3.43	1.63	0.52	0.70	0.03	0.27

Table 4
Trace element contents in deposited dust (DD, <500 μm) and channel profile (CP) samples. Values in $\mu g \cdot g^{-1}$. Mo, Cd, Ta, Tl and Bi were found in concentrations lower than detection limit (<dl). *TH, Tailings handling; CWF, Coal working front; RT, Road traffic into a mine road for tailings.*

Sample	Zone	Li	Be	B	Sc	Ti	V	Cr	Mn	Co	Ni	Cu	Zn	Ga	Ge	As	Se	Rb	Sr	Y	Zr	Nb	Sn	Sb	Cs	Ba	Hf	W	Pb	Th	U	REE
BNW_DD_002_CWF	C	8.0	<dl	55	5.2	1265	42	20	86	4.7	10	22	100	6.1	1.1	3.6	2.0	15	320	12	30	2.2	1.1	<dl	1.3	397	1.4	<dl	6.6	1.7	1.2	60
BNW_DD_012_CWF	C	4.6	<dl	39	2.1	794	16	10	66	2.9	8.7	7.7	34	3.1	<dl	1.9	<dl	8.9	190	4.5	18	1.6	0.77	<dl	0.74	344	0.86	<dl	2.7	1.0	3.2	21
BNW_DD_005_CWF	C	1.1	<dl	64	<dl	138	2.5	2.2	17	<dl	2.0	3.0	25	<dl	<dl	<dl	<dl	1.4	413	0.92	3.1	<dl	<dl	<dl	<dl	349	<dl	<dl	<dl	<dl	<dl	4.0
BNW_DD_006_CWF	D	1.5	<dl	54	<dl	64	1.2	1.2	31	<dl	1.7	2.8	27	<dl	<dl	<dl	<dl	<dl	289	<dl	1.7	<dl	<dl	<dl	<dl	1022	<dl	<dl	<dl	<dl	<dl	1.6
BNW_DD_013_CWF	D	2.6	<dl	61	<dl	196	3.9	2.7	22	<dl	2.8	5.1	22	0.86	<dl	<dl	<dl	2.1	398	1.3	3.8	<dl	<dl	<dl	<dl	406	<dl	<dl	1.0	<dl	<dl	5.2
BNW_DD_007_CWF	E	0.78	<dl	58	<dl	89	2.7	1.7	282	<dl	2.0	3.2	21	<dl	<dl	0.90	0.81	<dl	82	1.1	2.0	19	4.3	<dl	<dl	420	<dl	<dl	0.91	2.1	2.1	2.5
BNW_DD_001_TH	A	23	1.1	29	16	7735	158	108	65	40	80	53	116	27	2.6	6.3	3.4	62	88	19	172	19	4.3	1.5	5.5	328	8.1	1.7	24	14	4.4	135
BNW_DD_010_TH	B	17	0.76	11	9.5	3755	69	49	1448	13	22	17	80	13	2.2	3.0	4.5	44	320	25	82	6.0	1.6	2.4	2.1	447	4.2	<dl	9.3	3.9	1.4	130
BNW_DD_011_TH	B	30	1.7	25	15	5300	112	68	307	14	32	36	93	19	2.5	5.9	3.1	75	130	28	115	8.8	2.4	0.82	5.2	499	5.8	<dl	12	6.1	2.1	146
BNW_DD_003_TH	B	29	1.6	12	14	5566	108	80	427	14	38	27	95	18	2.3	10	3.6	66	111	28	112	8.7	2.2	4.4	4.4	470	5.6	<dl	11	5.6	1.6	139
BNW_DD_004_TH	B	32	1.6	14	14	5254	111	82	463	14	36	28	94	19	2.4	10	4.3	66	108	28	113	6.7	2.2	<dl	4.5	358	5.4	<dl	11	5.8	1.7	141
BNW_DD_008_TH	F	22	1.5	133	17	5613	125	69	217	28	55	43	112	20	3.2	16	4.1	71	327	30	124	9.8	2.7	1.1	5.7	495	6.0	0.73	19	6.3	2.2	148
BNW_DD_009_RT	G	25	2.1	30	14	5253	109	66	250	14	31	32	102	19	2.8	8.6	3.1	72	166	28	114	9.2	2.4	0.9	4.8	466	5.6	<dl	13	6.0	2.9	138
BNW_CP_001	C	1.2	<dl	67	<dl	59	1.3	1.8	26	<dl	1.9	2.6	20	0.38	<dl	<dl	<dl	<dl	223	<dl	1.2	<dl	0.44	<dl	<dl	280	<dl	<dl	<dl	<dl	<dl	1.4
BNW_CP_002	D	<dl	<dl	56	<dl	31	<dl	0.86	19	<dl	1.9	2.2	17	<dl	<dl	0.49	<dl	<dl	238	<dl	0.69	<dl	<dl	<dl	<dl	106	<dl	<dl	<dl	<dl	<dl	<dl
BNW_RDD_002_CWF	C	6.6	1.9	25	5.4	1150	35	16	66	4.4	7.8	17	34	5.7	<dl	2.8	1.3	14	316	10	42	3.1	0.95	<dl	1.3	105	<dl	<dl	4.5	2.4	1.2	63
BNW_RDD_005_CWF	C	2.3	<dl	62	<dl	180	4.2	3.1	19	<dl	3.7	3.1	17	<dl	<dl	1.8	<dl	2.1	886	1.2	7.1	<dl	<dl	<dl	<dl	59	<dl	<dl	1.20	<dl	<dl	5.3
BNW_RDD_006_CWF	D	2.1	<dl	53	<dl	58	1.3	1.9	33	<dl	1.9	2.6	18	<dl	<dl	7.1	<dl	<dl	319	<dl	1.2	<dl	<dl	<dl	<dl	39	<dl	<dl	1.30	<dl	<dl	1.9
BNW_RDD_007_CWF	E	<dl	<dl	76	<dl	99	3.1	2.5	380	<dl	4.8	15	39	<dl	<dl	1.7	<dl	<dl	91	1.3	4.0	<dl	<dl	<dl	<dl	17	<dl	<dl	2.7	<dl	2.4	4.2
BNW_RDD_001_TH	A	29	1.2	369	19	7323	194	112	52	44	85	52	139	30	1.9	7.8	1.3	76	87	16	262	16	4.1	1.3	6.6	246	4.8	<dl	33	14	5.1	120
BNW_RDD_003_TH	B	35	<dl	57	17	5842	142	80	531	18	59	35	118	20	2.8	13	3.7	75	155	31	173	6.5	3.2	1.5	5.1	464	4.8	<dl	17	6.5	1.8	148
BNW_RDD_008_TH	F	20	1.7	69	14	5457	138	62	138	27	56	64	108	21	2.2	29	3.6	71	405	26	156	9.5	3.9	3.4	5.5	456	4.3	0.92	21	6.6	2.2	140
BNW_RDD_009_RT	G	30	<dl	<dl	16	5549	130	73	198	16	34	55	174	20	2.3	9.5	3.9	73	162	25	144	8.2	7.5	26	5.7	326	3.9	<dl	19	5.6	3.6	131

Table 5
50 and 90 percentile values (D50 and D90, in μm) of the grain size distribution of the respirable deposited dust (RDD). *TH, Tailings handling; CWF, Coal working front; RT, Road traffic into a mine road for tailings.* ** Not enough sample to complete the analysis.

Name	Zone	Activity	D50	D90
BNW_RDD_002	C	CWF bottom open-pit (DD on car)	3.3	7.3
BNW_RDD_005	C	CWF bottom open-pit (extraction coal & truck uploading by excavator)	3.5	7.7
BNW_RDD_006	D	CWF bottom open-pit (extraction coal & truck uploading by excavator)	3.1	7.3
BNW_RDD_007	E	CWF bottom open-pit (truck uploading by excavator)	4.0	7.5
BNW_RDD_001	A	TH, gangue (truck uploading by excavator)	2.2	4.4
BNW_RDD_003	B	TH, drilling into gangue	3.2	4.5
BNW_RDD_008	F	TH, gangue dust	**	**
BNW_RDD_009	G	RT, trucks in a gangue extraction road	**	**

samples make them potentially more hazardous for the coal workers (Borm, 2002; Gilmour et al., 2004; Li et al., 2008, 2003; Oberdörster et al., 1992).

Tables 2 to 4 summarise the results of the mineralogical and geochemical characterisation of RDD samples. The concentration of minerals and elements is compared using the RDD/DD ratio. Clays and calcite are consistently enriched in the finer DD fraction (RDD/DD 1.1–1.4), similar to the quartz in the road traffic and gypsum, and microcline in the tailings handling (1.1, 1.6 and 1.1 respectively) (Fig. 3). Anatase, plagioclase, and quartz in the coal working front and tailings handling, and gypsum in the coal working front and road traffic RDD were consistently coarser (RDD/DD 0.1–0.9) (Fig. 3). Similar results were obtained by Johann-Essex et al. (2017), who analysed respirable dust samples from different underground coal mines and their mineral content increase with the distance to the coal working front.

For major elements, most RDD/DD values lay within the range of 0.8–1.2 (Fig. 4). However, in the coal working front zone, relative Fe content decreased in the RDD (<0.8) whereas Mg, Al, and P (all occurring mostly in phosphates and clay minerals) increased (>1.2), similar to Ca and P in the tailings handling zone (Fig. 4). In the road traffic zone, Na content decreased in the RDD (<0.6). For trace elements, RDD/DD ratios >1.2 were found for Nb, Th, Cr, Sr, Li, As, Pb, Cu, Zr and Ni in the coal working front, whereas ratios were < 0.8 for Se, Hf and Ba (Fig. 5). The finer character of the first group of elements is likely

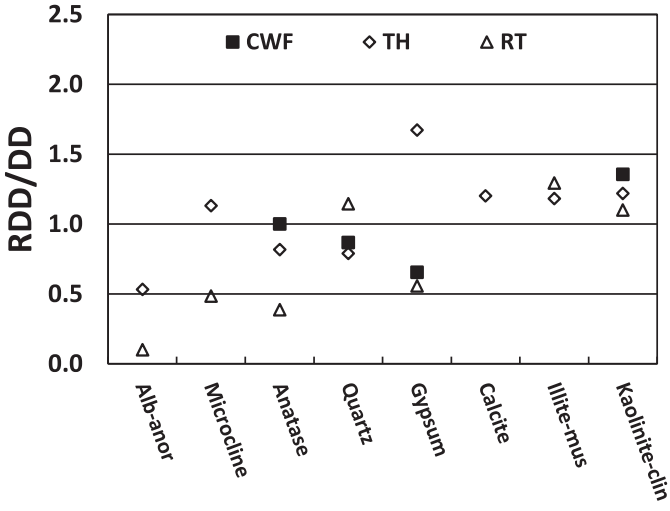

Fig. 3. Ratio of mineral contents determined by XRD analysis in the respirable deposited dust (RDD) and their parent deposited dust (DD, <500 μm) (RDD/DD). Average for each type of DD: *TH, tailings handling; CWF, Coal working front; RT, Road traffic into a mine road for tailings.* Values used are shown in Table S1.

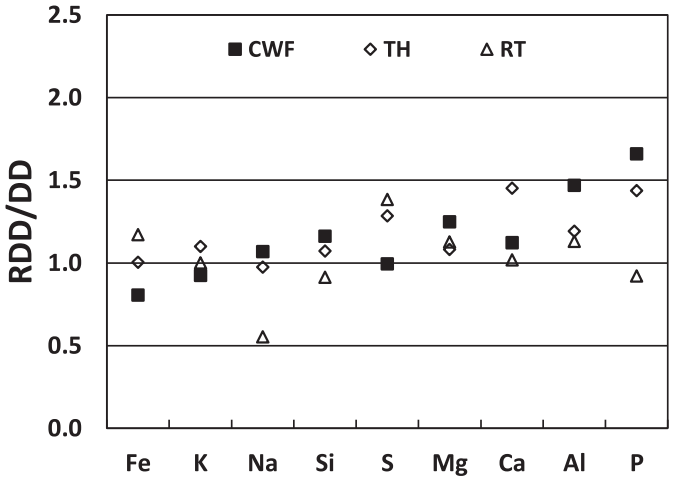

Fig. 4. Ratio of major element contents in the respirable deposited dust (RDD) and their parent deposited dust (DD, <500 μm) (RDD/DD). Average for each type of DD: *TH, Tailings handling; CWF, Coal working front; RT, Road traffic into a mine road for tailings*. Values used are shown in Table S2.

attributed to their association with clays and carbonates and perhaps with mining machinery wear (Fig. S4 c) (Azam and Mishra, 2019; Moreno et al., 2019; Querol et al., 2007). In contrast, the coarser Ba pattern might be due to the occurrence of fine barite ($BaSO_4$) crystals embedded in the coaly matrix (evidenced by fig. S4 d) (Gürdal, 2008; Zhao et al., 2014). Notables are the contrasting size patterns of Zr and Hf, which is attributed to the presence of both geogenic zircon (coarser, enriched in Hf) and contamination from the wear of drilling and other mining machinery (finer and poorer in Hf: fig. S4, e-f). For the tailings handling RDD samples, RDD/DD ratios were > 1.2 for W, As, Zr, Sn, Cu and Sb and < 0.8 for Ge, Se and B and the road traffic RDD Cu, Sn, Pb, Zr, Sb, Zn and Se, and Ba and Hf, respectively (Figs. 5, S4, f-h).

An enrichment (not extraordinarily high but clearly evident) of elements of potential concern in the RDD versus the parent materials (represented by DD in coal working fronts and tailings handling operations) was evident. Accordingly, RDD constituents and health effects might be quite different to what would be expected if the constituents and related effects from the parent materials are simply extrapolated without considering the effects of mineral fractionation within the dusts released during the coal mining process.

4.1.5. *Oxidative potential of the respirable deposited dust*

Oxidative potential is suggested to be one of the most relevant indicators of PM toxicity. The OP values obtained for the RDD samples (Table 6) were relatively low compared to those obtained in a prior study of RDD originating from underground mines of other coal mining districts with substantially higher pyrite contents (Trechera et al., 2020). Thus, OP^{AA} in this study ranged from 0.1–0.5% AA consumption·μg^{-1} RDD, while in the referred study, 0.4–2.0%·μg^{-1} was reached in 11 out of 13 RDD samples (Table 6). For OP^{GSH}, the results were the opposite, with 0.2–0.4%·μg^{-1} in this study and 0.0–0.2%·μg^{-1} in the underground mines (Table 6). Furthermore, in this study, 27–63% of the OP^{TOT} was supplied by the OP^{AA}, while this contribution in RDD samples from underground mines reached 80–100%.

The OP^{TOT} (OP^{AA} + OP^{GSH}) potential obtained for RDD in this study (0.34 to 0.80 OP^{TOT} %·μg^{-1}) is slightly lower or similar to urban dust (NIST control 1.0 OP^{TOT} %·μg^{-1}) and from indoor and outdoor locations around a Fe-ore facility in Iran (0.9 $OP^{TO\ T}$%·μg^{-1}, Soltani et al., 2018). However, it is much lower than those obtained for PM from the Chamonix Valley (France) in summer (1.4 OP^{TOT} %·μg^{-1}) and winter (4.1 OP^{TOT}%·μg^{-1}) (the latter with PM contributions from biomass burning) (Calas et al., 2018) and PM from subway platforms from Barcelona (2.5 OP^{TOT} %·μg^{-1}, Moreno et al., 2017).

A cross-correlation analysis using r coefficients was carried out using the OP^{AA} and OP^{GSH} values of each RDD sample with the content of major and trace elements and minerals in the respective samples (Fig. 6). When using the 8 RDD samples from the open-pit (Fig. 6a), it was shown that the contents of Mn, followed by those of anatase and calcite, drove the OP^{AA} (group I in the figure and r = 0.8–0.9 with OP^{AA}). Those of gypsum and moisture and a relatively coarse 10 percentile of the PSD drove the OP^{GSH} (r = 0.5–0.7, group II in the figure).

When considering only the RDD samples from the coal working front (Fig. 6), a marked correlation between OP^{AA} and OP^{GSH} was obtained (r = 0.8). In this case, moisture (Fig. 6b) and gypsum contents drove OP^{AA} (r = 0.5–0.6, group I) and Ni and Pb concentrations drove OP^{GSH} (r = 0.7–0.8, group II). Furthermore, a coarser 25 percentile of the PSD and the contents of anatase, Mn, U, Zn and Cu drove both OP^{AA} and OP^{GSH} (r = 0.6–1.0, group III). Conversely, elevated contents of Mg, Sr and Ca were associated with a decrease in both types of OP (r = −0.5 to −0.8 with both OP types, group IV). Despite these high r coefficients, average OP^{AA} values of the coal working front RDD samples were low (0.2%·μg^{-1}), compared to the tailings handling and road traffic RDD samples (0.3%·μg^{-1}, and much lower than those of the RDD from underground coal mines (0.70%·μg^{-1}, Trechera et al., 2020) with much greater pyrite contents. For OP^{GSH} the situation was reversed, with samples yielding 0.3, 0.2 and 0.1%·μg^{-1}, respectively.

The RDD from tailings handling and road traffic, also with relatively low OP^{AA}, was driven by the contents of multiple silicate- and calcite-associated elements, Mn and anatase, and a finer 25 percentile of the PSD (r = 0.6–1.0 and − 0.8 for the latter, group I in Fig. 6c). For OP^{GSH}, contents of As, Bi, Be, Sr, S and moisture were found to be positively

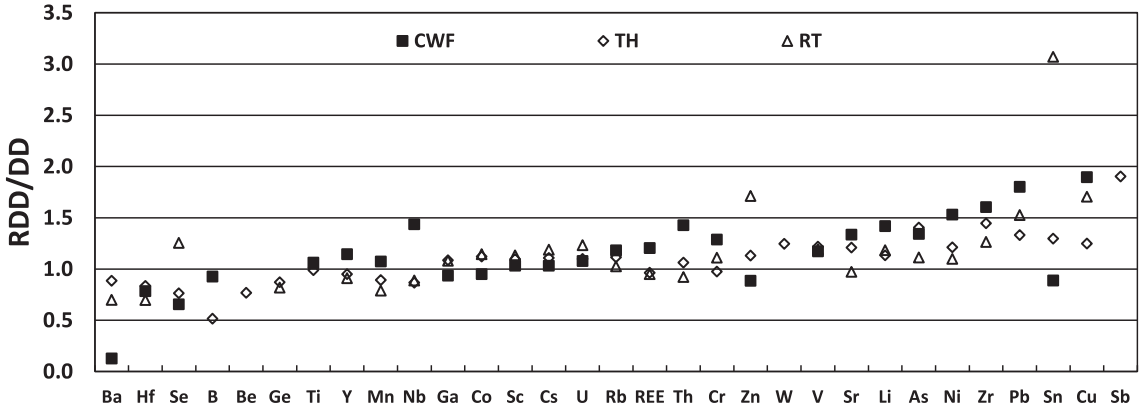

Fig. 5. Ratio of trace element contents in the respirable deposited dust (RDD) and their parent deposited dust (DD, <500 μm) (RDD/DD). Average for each type of DD: *TH, tailings handling; CWF, Coal working front; RT, Road traffic into a mine road for tailings*. Values used are shown in Table S3.

Table 6
Oxidative potential (OP) values of respirable deposited dust (RDD) in %consumption·μg^{-1} for Ascorbic Acid (OP^{AA}), Glutathione (OP^{GSH}) and Total oxidative potential (OP^{TOT} = OP^{AA} + OP^{GSH}). *TH, Tailings handling; CWF, Coal working front; RT, Road traffic into a mine road for tailings*. On the bottom, results of previous studies from different underground coal mines in China (Trechera et al., 2020).

Name	Zone	Activity	OP^{AA}	OP^{GSH}	OP^{TOT}
BNW_RDD_002	C	CWF bottom open-pit (DD on car)	0.13	0.35	0.48
BNW_RDD_005	C	CWF bottom open-pit (extraction coal & truck uploading by excavator)	0.10	0.20	0.40
BNW_RDD_006	D	CWF bottom open-pit (extraction coal & truck uploading by excavator)	0.11	0.23	0.34
BNW_RDD_007	E	CWF bottom open-pit (truck uploading by excavator)	0.40	0.40	0.80
BNW_RDD_001	A	TH, gangue (truck uploading by excavator)	0.20	0.20	0.40
BNW_RDD_003	B	TH, drilling into gangue	0.50	0.20	0.80
BNW_RDD_008	F	TH, gangue dust	0.23	0.24	0.47
BNW_RDD_009	G	RT, trucks in a gangue extraction road	0.18	0.17	0.35
Underground mines (Trechera et al., 2020)					
BCC_RDD_011	Mine 1	300 m CWF#7	1.2	0.0	1.2
BCC_RDD_009	Mine 1	100 m CWF#7	2.0	0.2	2.2
BCC_RDD_008	Mine 1	50 m CWF#7	0.9	0.0	0.9
BCC_RDD_005	Mine 1	CWF#7	0.8	0.1	0.9
BCC_RDD_014	Mine 1	CWF#11	0.1	0.0	0.1
BCC_RDD_001	Mine 1	Gallery close CWF#7 (cemented)	0.7	0.5	1.2
BCC_RDD_015	Mine 1	Floor train wagons	0.2	0.0	0.2
SCC_RDD_001	Mine 2	2000 m CWF	0.6	0.0	0.6
SCC_RDD_004	Mine 2	100 m CWF	0.5	0.1	0.6
SCC_RDD_005	Mine 2	CWF	0.5	0.2	0.6
SCC_RDD_007	Mine 2	Coal milling	0.4	0.1	0.5
BSC_RDD_001	Mine 3	Abandoned mine 30 m CWF	0.7	0.1	0.7
BSC_RDD_002	Mine 3	Abandoned mine 90 m CWF	0.5	0.1	0.6

correlated (r = 0.6–0.9, group II). Those of Ba and P were correlated with both OP types (group III, r = 0.5–0.7), and Zn, Sb, Sn and U were negatively correlated ($r = -0.4$-0.9, group IV).

According to the results, Mn and anatase were found to be major drivers of OP^{AA}, and OP^{GSH} in the RDD from the coal working front, while for tailings handling-road traffic a finer particle size was associated with a high OP^{AA}. In the first case, Mn and anatase occur in this type of RDD, mostly embedded in the coal matrix (Fig. S4, f, j–l), and this might cause enrichment in the coarser dust particles compared to the finer ones.

The OP^{GSH} of the tailings handling-road traffic RDD samples was found to be driven by moisture and elements usually associated with sulphate minerals from the weathering of sulphides (As, S, Ba, Sr) and, in the coal working front, by some heavy metals and U (in addition to Mn and anatase). Thus, in the case of DD from the coal front, the impact of Mn and anatase on both OP^{AA} and OP^{GSH} was implicated in the correlation between both OPs, but this was not the case for the samples from tailings handling-road traffic.

Fig. 6d shows the above mentioned OP^{AA} and OP^{GSH} cross-correlation analysis for a set of 21 RDD samples, 8 from the coal open-pit mine of this study and 13 from three underground mines by Trechera et al. (2020). This analysis shows that OP^{AA} was clearly driven by contents of Fe-sulphates, other sulphates and anatase, as well as by a slightly coarser PSD (probably favoured by the occurrence of Fe-sulphates) (group I and r = 0.7–0.9). Because of the high quality of the coal mined in the open-pit, the low content of pyrite might account for lower Fe-sulphates, oxides and metal contents in RDD, and accordingly for the lower OP compared with the other RDD samples from other mines. Fe-oxides and sulphates derived from the oxidation of pyrite were suggested as significant drivers of OP in coal mine dust, and probably contributing to CWP injuries in coal mine workers (Huang et al., 2005). Also, as stated by Trechera et al. (2020), acid mine drainage favoured by underground mining might also favour the oxidation of sulphides. The presence of anatase was a major OP^{AA} driver in this study: the lung-inflammation-related toxicity of inhaled TiO_2 particles is well documented (Oberdörster et al., 1992; Schins and Borm, 1999).

On the other hand, OP^{GSH} is moderately driven by moisture, Ca and Na contents (r = 0.5), probably representing the amount of coaly matrix and sulphate and carbonate minerals. The very low ash yield and the relatively high Mn contents of the coals of this study might account for an increased OP^{GSH,} compared to the underground RDD samples.

Based on these results, a multilinear-regression analysis was applied to the 21 RDD data set using the above OP drivers and represented the OP^{AA} and OP^{GSH} according to Eqs. (13) and (14).

$$\mathrm{OP}^{AA}\ (\%\mu g^{-1}) = 0.211{*}\mathrm{anatase}\ (\%db) + 0.055{*}\mathrm{sulphate}\textit{minerals}\ (\%db) + 0.147\ (r = 0.93 p = 0.00) \quad (13)$$

$$\mathrm{OP}^{GSH}\ (\%{\cdot}\mu g^{-1}) = 0.066{*}\mathrm{moisture}\ (\%ad) + 0.026{*}\mathrm{Ca}\ (\%db) + 0.067\ (r = 0.70, p = 0.00) \quad (14)$$

Fig. 7 shows the outputs of the multilinear regression with the differentiation of mines from which RDD samples were obtained. The role of drivers of OP in specific RDD samples (such as Mn in this study) with a specific composition (low metal and sulphur sediments in this study) is diluted when compiling data from different mines where drivers such as pyrite oxidation products and anatase seem to prevail.

4.2. Online and offline air quality measurements in the open mine pit

4.2.1. Online measurements of air quality

As stated in the methodology section, levels of PM_{10}, $PM_{2.5}$, BC and UFP were measured near specific mining activities, where, in addition, DD was simultaneously sampled.

4.2.1.1. Tailings handling. In zone A, air quality around coal gangue uploaded on a truck with an excavator was monitored (16/10/2018, 11:45–12:55 h LT). Here, the impact of emissions from the loading of tailings on trucks and the exhaust emissions from diesel excavators and natural compressed gas trucks on UFP, BC and PM levels and DD were evaluated. This zone was located at a relatively high altitude in the upper banks at the SW of the open mine pit (Fig. 1C). There, because few operations take place, wetting of the surfaces or other dust abatement controls were not implemented. The gangue loaded was a clear pale beige clay-rich material, probably transported to processing plants to be used in the ceramic industry. The very clear colour indicates a minimal amount of coaly material, meaning that absorbance from the BC was hardly influenced by dust. The RDD fraction from this operation (BNW_RDD_001_TH, Table 2) was composed of 74, 9.7, 15, 0.3, 0.6, 0.3, 0.3% clay minerals kaolinite/clinochlore, illite/muscovite, quartz, albite/anorthite, calcite, gypsum and anatase, respectively. The DD sampled was very fine with 55, 38 and 26% of DD10, DD4 and DD2.5 in DD500, and 98% of DD500 in DD.

Fig. 8a shows the time series of 1 min concentrations of $PM_{2.5}$, BC

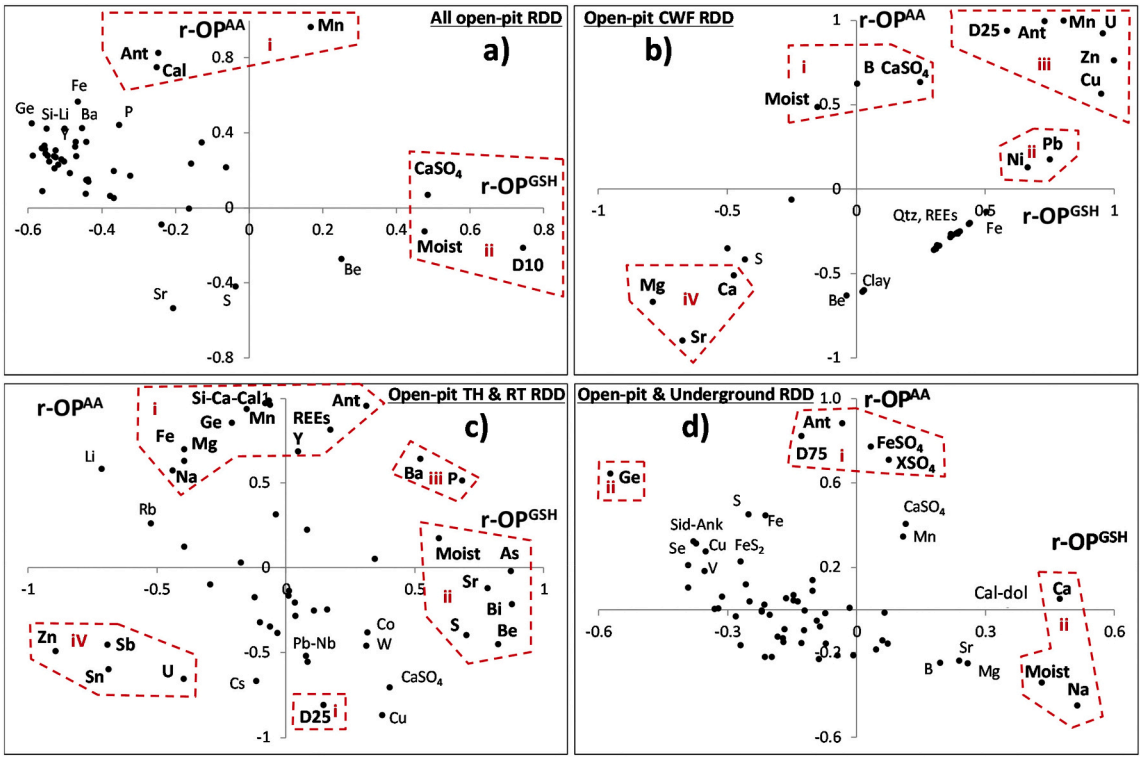

Fig. 6. Cross correlation plots between the Pearson's correlation coefficients of the normalised (concentration/average concentration) concentrations of the elements and minerals contents in the respirable deposited dust (RDD) samples and their respective OP^{AA} and OP^{GSH} values using; a) Eight RDD samples from the open-pit coal mine; b) Four CWF RDD samples from the open-pit coal mine; c) Three TH RDD samples and one RT RDD sample from the open-pit coal mine; and d) Data from this study and 13 additional RDD samples from underground mining by Trechera et al. (2020) previous study. *TH, tailings handling; CWF, Coal working front; RT, Road traffic into a mine road for tailings.*

and UFP recorded at this site (with ambient conditions of 21 °C, RH 33%, and CO_2 428 ppm). Very elevated levels of PM_{10} and $PM_{2.5}$ (1 h average values of 3652 and 354 $\mu g \cdot m^{-3}$ for the personal PM_{10} PEM samplers, and $PM_{2.5}$-Dusttrack, respectively) were reached, with $PM_{2.5}/PM_{10}$ of 0.24. However, levels of UFP were relatively low, reaching an average of 4475 $\#cm^{-3}$, typical from a regional background or low polluted urban sites according to Cassee et al. (2011) and Morawska et al. (2008). Levels of BC (11 $\mu g \cdot m^{-3}$) can be considered moderate compared with typical concentrations measured in European, Middle East and Asian urban road traffic sites (maxima annual or seasonal averages of 8–18 $\mu g \cdot m^{-3}$, Hung et al., 2014; Hussein et al., 2019; Reche et al., 2011), especially given the fact that in this study measurements were collected near two large operating mining motor engines.

Emissions of PM_x mainly occurred during the loading of the excavator (with 1 min levels up to 1080 $\mu g \cdot m^{-3}$ $PM_{2.5}$). These are clearly correlated with BC peaks and, accordingly, are attributed to the engine of the excavator. However, UFP particles were completely decoupled from BC and PM, and peak concentrations are attributed to the exhaust emissions of the truck. Regardless, UFP peaks reached up to 11,000 $\#cm^{-3}$, which are relatively low considering the proximity to the truck, the low rpm of the stopped truck, and the fact that usually UFP averages reported for urban zones (Cassee et al., 2019; Morawska et al., 2008) are of the same order of the UFP peaks recorded at this mine site.

The impact of emissions from the drilling and working tailings with diesel excavators on levels of UFP, BC and PM and DD were also evaluated. Measurements were also performed close to drilling (16/10/2018, 12:28–13:40 h LT, 17 °C, RH 42%, CO_2 410 ppm) and excavator (17/10/2018, 12:28–13:40 h LT, 12 °C, RH 54%, CO_2 412 ppm) operations in zone B (Fig. S5a and b), also at the high altitude zones, but in this case at the N sector of the pit (12 °C, RH 54%, CO_2 412 ppm), and with no dust abatement measures implemented. There PM_{10} and $PM_{2.5}$ levels were reduced in relation to Zone A (1 h averages of 549 and 127, and 723 and 167 $\mu g \cdot m^{-3}$, respectively), with a similar $PM_{2.5}/PM_{10}$ ratio (0.23 in both cases). At that site, the mineral composition of the gangue RDD was 28, 56, 2.5, 12 and 1.1% clay minerals (74% of Kln/Clc and 10% of Ilt/Ms), quartz, feldspars, calcite and anatase. In this case, DD was much coarser than for the loading of gangue at A, with 18–28, 11–18 and 6–13% of DD10, DD4 and DD2.5 in DD500 and 80–97% of DD500 in DD.

4.2.1.2. Coal working fronts. Measurements and sampling were conducted in the coal working fronts at the bottom of the open-pit, where coal was worked and loaded onto trucks by excavators at zones C (S sector) and D (SE). These were also carried out at a mid-altitude sector E (central area), where coal was worked with excavators without loading onto trucks. At these sites wetting of the surface was frequently applied to abate dust resuspension. Here, the impact of emissions from coal working with diesel excavators, the loading of coal on trucks, the emissions from resuspension of dust by trucks accessing and leaving the front, and the exhaust emissions of excavators and trucks on UFP, BC and PM levels and DD were evaluated.

During coal work and loading, RDD sampled at these three sites was found to be greatly enriched in the organic coal matrix (75–95, 0–12, 0.5–12, 0–3, 0.3% coal, clay minerals, quartz, gypsum and anatase, respectively), as the coal worked is very low in ash yields. The DD of the three positions is markedly coarser (probably due to the low ash yields) than the one from the gangue, with DD10, DD4, DD2.5 accounting for 19–32, 9–15 and 5–9% of DD500, and DD500 for 64–100% of DD.

At the working front sites (zone C and D), where coal is extracted and loaded, sampling and measurements were performed on 16/10/2018 at 14:06–15:45 h LT, in sector C, and, 16:27 to 17:32, sector D, under environmental conditions of 19 °C, RH 44%, and CO_2 450 ppm. Average PM_{10} and $PM_{2.5}$ levels reached 1535 and 98 $\mu g \cdot m^{-3}$, respectively, at site C, and, 264 $\mu g \cdot m^{-3}$ $PM_{2.5}$ at site D. The $PM_{2.5}/PM_{10}$ ratios were very low

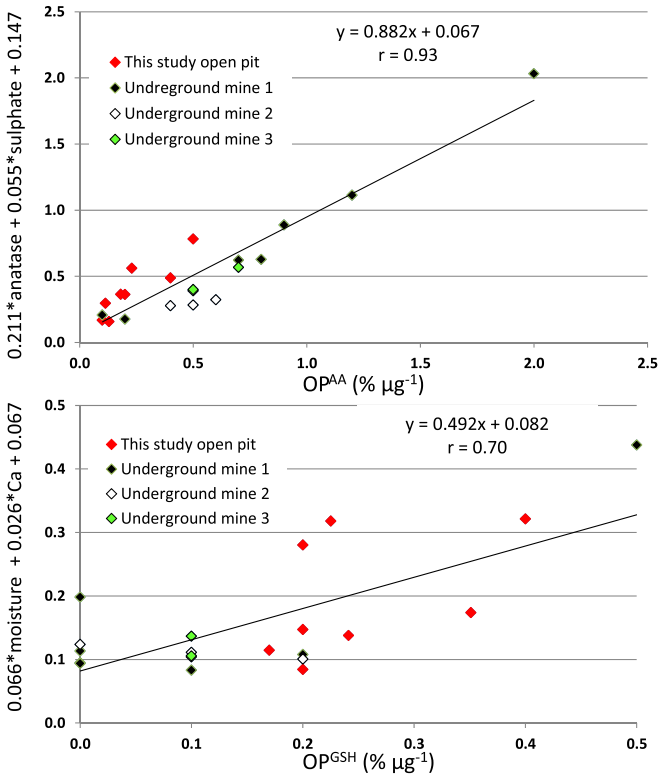

Fig. 7. Cross correlation plots between OP^{AA} and OP^{GSH} multilinear regression with their respective geochemical drivers, combined with underground mine data on RDD (mines 1 to 3) from previous study by Trechera et al. (2020).

(0.06). Levels of BC were moderate (22 and 9 µg·m^{-3} for C and D sites, respectively) considering the number of trucks and excavators and the potential influence of coal mine dust on absorbance measurements of BC. However, levels of UFP, similarly high at the C and D positions, reached average concentrations of 31,682 and 25,735 #cm^{-3}, respectively. These are typical values of urban traffic sites (Morawska et al., 2008), but unexpectedly low for this busy mining environment. Regardless, UFP were markedly higher than those recorded at the highest altitude sectors of the mine where the work was done with tailings. This is attributed to the elevated truck traffic and excavator density and lower dispersion (because sectors C and D are at the bottom of the large open-pit). Thus, as shown in Fig. 8b and c, background and peak levels reached 11,000–17,000 #cm^{-3}, and up to 111,300 #cm^{-3}, one order of magnitude greater than at zone A (close to the top of the open-pit). Also, as shown in the figure, PM and BC peaks again coincided due to the impact of the emissions from the engines of the excavators (BC) and those during loading. However, UFP peaks were closely related to the Liquefied-Natural-Gas fuelled truck exhaust emissions.

At the mid-altitude coal working front area with no truck loading activity (zone E), measurements around coal works with an excavator (17/10/2018, 10 °C, RH 64%, CO_2 395 ppm), yielded moderately low PM_{10} and $PM_{2.5}$ levels (68 and 28 µg·m^{-3}, respectively), and high $PM_{2.5}$/PM_{10} ratios (0.37) (Fig. S5 c).

4.2.1.3. Truck traffic into the open-pit. At the border of mine track located at a relatively high altitude, on 17/10/2018, 11:32 to 12:46 h LT, with ambient conditions of 12 °C, RH 55%, CO_2 391 ppm. In this track, there was frequent wetting of the surface to abate resuspension of dust by truck movement. Here, the impact of emissions from the loss of bulk material from trucks, the road dust resuspension, and the exhaust emissions from loaded trucks on UFP, BC and PM levels and DD were evaluated.

Respirable deposited dust sampled at this site was composed of 16, 82, 2, 1 and 0.3% of clay minerals, quartz, feldspar, gypsum and anatase, 36, 23 and 15% DD10, DD4 and DD2.5 in DD500, and 97% of DD is DD500. Thus, this dust, compared to that from coal front or tailings areas, is intermediate in size and greatly enriched in quartz. Fig. 8c shows that levels of BC (9 µg·m^{-3}) and $PM_{2.5}$ (264 µg·m^{-3}) were moderate-low compared to those at other sites due to the intermittent emissions and the relatively high dispersive conditions that prevail at the site. Trucks are fuelled with Liquefied-Natural-Gas, and very low BC levels, but relatively high UFP concentrations (22,775 #cm^{-3}) were recorded, although values were still moderate compared to traffic sites. Relevant UFP emissions are supported by a previous study that examined the UFP emissions from natural gas-fuelled heavy-duty vehicles (Giechaskiel, 2018). These results are very close to the ones by Kurth et al. (2014) in coal mining areas influenced by emissions from machinery and trucks (mostly 5000 to 10,000 #cm^{-3}, but reaching 30,000 #cm^{-3} in some of them).

The high quartz content and RDD contents measured at the border site of a mine track suggest the possibility of quite hazardous exposure in this area. However, workers rarely are exposed to these conditions because only trucks and excavators work there, and these are indoor ventilated with filtered air. Also, the DD loads are visibly lower than in other locations.

The bottom of the open-pit, where coal is primarily worked, had moderate-high PM levels probably due to the application of control measures (surface wetting). The PM at this site was coarser than in other locations because the coal mined is of high quality (low S and ash yield) and coal fragments are coarser than the mineral ones. Peak concentrations of BC seem to be associated with those of PM but not to UFP. This evidence suggests that the exhaust of the excavators extracting and loading coal is the main source of BC, but mean levels are typical of those from high-traffic sites in busy cities (Reche et al., 2011). The tailings are disposed of in the upper parts of the open-pit but, in some cases, these are discarded with no control measures, and high levels of PM were measured when loading high clay materials. The ambient air in the mine track for extraction of tailings in the upper part of the pit was characterised by low BC, moderate PM and high UFP concentrations, due to the high ventilation and the fact that trucks are fuelled with natural gas (Fig. 8c). Notably, at the bottom of the mine, due to heightened excavator and truck density but lower atmospheric dispersion, UFP levels are one order of magnitude higher than at the top of the pit. These are also above the highest PM levels recorded close to the handling of tailings at the banks in that location.

4.2.2. PM_{10} levels and composition

Sampling of PM_{10} was carried out in some of the locations simultaneously with the sampling of DD. Table 7 summarises the ambient air PM_{10} concentrations of major and trace elements (in µg·m^{-3} and ng·m^{-3}, respectively), and, Table S2 shows the ambient air PM_{10} details of collection from the different zones of the open-pit mine.

The coal working front PM_{10} contained a markedly elevated proportion of coal (90–95%), much higher than road traffic and tailings handling PM_{10} samples (10–35%). Comparing the PM_{10} compositions with those of RDD obtained from DD co-collected at the same zones, and, taking into account that the first refers to PM with at least 50% <10 µm and the second to <4 µm, remarkable similarities were found. This result is notable because DD is much easier and cheaper to sample than PM_{10}. However, remarkable PM_{10}/RDD differences were found in the road traffic only for Zn, Cu, As, Cd and Sn, whose contents were much higher in PM_{10} than in RDD. These differences might be due to the high machinery and brake and tyre wear emissions at road traffic, as these elements in PM_{10} are usually attributed to these specific emission sources (Amato et al., 2009). However, due to their relatively fine size, their deposition rate is low and accordingly depleted in RDD compared with PM_{10}. Moreover, Liang et al. (2006) show China occupational exposure limits (OELs) for permissible concentration-short term exposure limit (PC-STEL) for coal dust with less content of 10% in SiO_2 (3.5 mg·m^{-3})

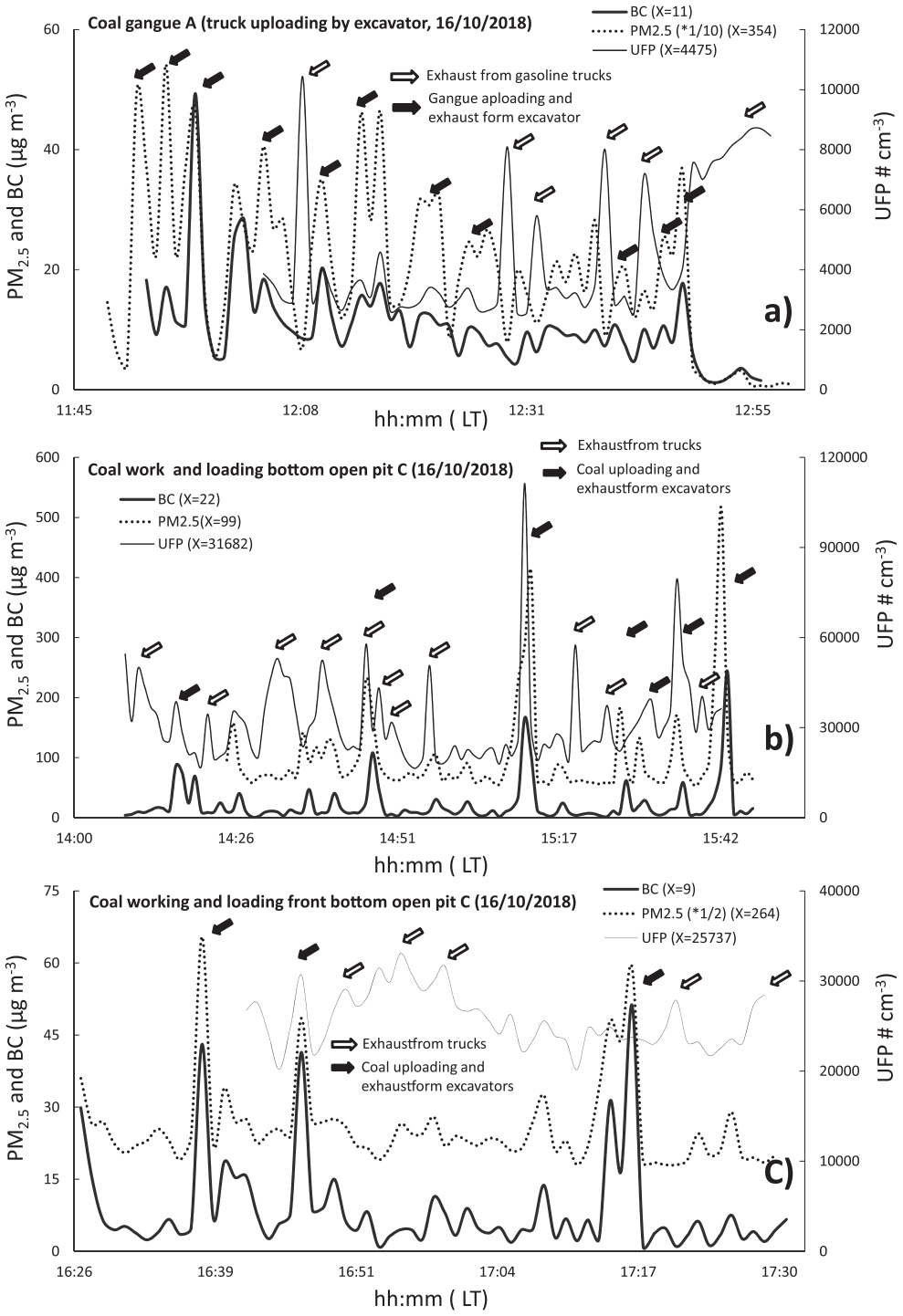

Fig. 8. Ambient concentrations of BC, $PM_{2.5}$ and UFP measured in the vicinity of tailings handling, coal working front and road traffic into a mine road for tailings.

and for the content between 10 and 50% in SiO_2 (1.0 mg·m^{-3}). In the coal working front measurements recorded a concentration of 1.4 mg·m^{-3} with less 10% content of SiO_2. In the tailings handling and road traffic concentration values were 2.7 and 0.1 mg·m^{-3} respectively (10–50% content of SiO_2).

5. Discussion and conclusions

In this study the mineralogy and geochemistry of deposited dust (DD) coal mine samples were examined, and their respirable DD (RDD) size fraction (<4 μm), collected from three different regions of an active, highly volatile bituminous open-pit coal mine. The areas of collection were coal working fronts, tailings handling sites, and road traffic sites. Online measurements of ambient air concentrations of particulate matter (PM_{10} and $PM_{2.5}$), black carbon (BC) and ultrafine particle numbers (UFP) were performed in the three mine zones. The respirable fraction samples were subjected to analysis of specific biological response or toxicological indicators (Oxidative Potential, OP). The results demonstrated i) a notable difference in particle size and chemical composition of DD from the different sampling areas, ii) a noticeable effect of moisture content and ash yield of DD on the particle size distribution (PSD), and, accordingly, on the potential emissions of the finer,

Table 7
Major and trace elements concentrations of coal dust exposure in open-pit coal mine. *TH, Tailings handling; CWF, Coal working front; RT, Road traffic into a mine road for tailings.* See Table S2 for sampling explanation.

Sample	CHI_1	CHI_2	CHI_4	CHI_6
Location	TH	CWF	CWF	RT
Zone	A	C	D	G
Concentration (ug/m^3)	3652	1535	29,179	257
	ug·m^{-3}	ug·m^{-3}	ug·m^{-3}	ug·m^{-3}
Tot	2719	1444	22,816	117
Coal	272	1335	21,104	41
Sum	2447	108	1711	76
SiO_2	1353	32	623	30
Al_2O_3	902	18	268	15
CaO	33	32	363	17
Fe_2O_3	29	4.4	44	5.5
K_2O	53	2.2	24	2.2
MgO	16	6.2	227	2.6
Na_2O	1.1	0.33	1.4	0.47
P_2O_5	1.9	0.57	2.3	0.80
S	15	10	123	0.54
TiO_2	39	0.82	12	1.1
	ng·m^{-3}	**ng·m^{-3}**	**ng·m^{-3}**	**ng·m^{-3}**
Li	71	6.6	58	1.0
V	587	16	159	20
Cr	337	17	77	1.0
Mn	196	89	705	29
Co	147	5.9	28	1.0
Ni	326	19	28	1.0
Cu	126	1.0	63	483
Zn	1081	103	1302	671
Ga	101	2.8	29	2.2
As	1.0	1.0	9.1	30
Rb	208	9.2	84	12
Sr	320	294	14,891	33
Zr	1111	276	692	279
Nb	50	1.0	18	1.0
Cd	1.0	1.0	1.0	108
Sn	53	19	101	96
Cs	19	1.0	8.3	1.0
Ba	673	124	4919	33
REE	424	22	240	14
Hf	39	13	25	13
Pb	114	31	64	31
Th	45	1.0	15	1.0
U	15	1.2	6.2	1.0

RDD fraction, iii) an enrichment of multiple elements (such as Nb, Th, Cr, Sr, Li, As, Pb, Cu, Zr and Ni) in this RDD fraction, attributed, at least in part, to mining machinery, tyre and brake wear emissions, iv) a major impact from specific mining operations and mine areas on the levels of air pollutants (such as high PM from tailings handling in the upper parts of the mine or the high UFP levels in the lower parts of the mine due to vehicle and machinery emissions and low dispersive conditions), v) the predicted low OP of the RDD fraction in a mine working with high-quality coal, with OP within the RDD fraction seemingly influenced by Mn, sulphates and anatase contents, as suggested by previous studies.

These results provide insight into the mineralogical and chemical variations present within inhalable size fractions of coal mine dust collected from differing localities within coal mines. The results show how, at the coal working front, the contents of mineral silicates in the inhalable fraction extracted from DD are much higher than in the parent coal. As would be expected from what is known about mineral matter in coals (e.g., Finkelman et al., 2019), the mineral silicates identified in this dust analysis at the coal working front are dominated by phyllosilicates (kaolinite/clinochlore) and quartz. In addition to which are sulphates (mostly gypsum) and very minor amounts of plagioclase feldspars and titanium oxide polymorphs such as anatase.

Perhaps the most important conclusion within this context is the fact that the data presented demonstrate that coals containing a greater content of fine aluminosilicates and silica impurities produce an elevated loading of finer, more deeply inhalable particles ($PM_{2.5}$) in resulting mine dust emissions than more carbonaceous samples, sourced from purer coals. Given the health concerns over the presence of siliceous particles in mine dust, it was observed that these can be preferentially fractionated into deeply inhalable size-fractions of PM, relevant to safe work practices. It follows that precautions for dust suppression and inhalation should be taken by miners working on coals with higher silicate impurity contents.

The mineralogy of dust generated at the coal working front is clearly quite different from that inhaled in the tailings handling and road traffic areas sampled. In these latter two environments, ambient dust contains a much higher concentration of silicates (quartz, feldspars, and clay minerals, with the phyllosilicate content including a significant quantity of illite-muscovite), plus notable amounts of carbonate and Ti-oxide (TiO_2), but much less sulphate. These mineralogical differences are reflected in the trace element content of the DDs, presumably reflecting the fact that most such elements are typically concentrated within phyllosilicates which are more abundantly present in the more felsic geochemistry of the tailings and road samples. Thus, the coal working front samples are depleted in most trace elements, notably Ti, V, Cr, Co, Ni, Ga, Ge, Se, Rb, Zr, Nb, Sn, Cs, Hf, Pb, Th, U, and REE. Such observations underline how coal mine dust has its own distinctive mineralogical, and therefore, geochemical signature, which is likely to be different from ambient PM encountered elsewhere in the mine.

From an exposure point of view, it is relevant to note that, in the coal working fronts, some elements (Nb, Th, Cr, Sr, Li, As, Pb, Cu, Zr and Ni) of the RDD were found at higher levels in the finer fraction than in the DD. This is possibly related to the mineralogy of the samples, since these elements are associated with clay and carbonate minerals, and also potentially with mining machinery wear. In contrast, the high levels of coarser Ba in DD might be due to the occurrence of fine barite ($BaSO_4$) crystals embedded in the coaly matrix.

Size patterns of Zr and Hf are also interesting, with 2 types of zircon likely present: the coarser (geogenic origin and enriched in Hf) and the finer (originating from the wear of the drilling and other mining machinery, lower in Hf). On the other hand, in tailings handling and road traffic, some elements (Cu, Sn, Pb, Sb and Zn) were associated with the RDD fraction and possibly produced from tyre and brake wear. Given the likelihood of enrichment of trace elements of potential concern in the finer, RDD fraction of the DD, when compared to the parent materials, it is necessary to emphasise the potential importance of size fractionation in mine dusts. It is not unreasonable to suspect that the health effects on mine workers breathing these particulate materials might be different to what would be expected if the composition of the dust derived from the parent materials was simply extrapolated, without considering the effects of mineral size fractionation in the dust released during the coal mining process.

When looking at the oxidative stress results obtained from the samples measured, the high coal quality of the open-pit coal mine, with its low pyrite and quartz contents (and therefore less potential risk of silicosis), appears to have minimised any obvious association of OP with acid mine drainage products. In particular, manganese and anatase were correlated with OP^{AA} and OP^{GSH} at the coal working front. In contrast, in the tailings handling and road traffic sampling areas, particle size was associated with OP^{AA}, which was negatively-correlated with the coal working front. This is due to the elements being likely embedded in the coal matrix, yielding slightly coarser particles. A clear correlation for RDD samples with sulphates and anatase was found in OP^{AA} and, to a lesser extent, with PSD. Also, a slight correlation was found between OP^{GSH} and Ca and Na contents, representing the amount of coaly matrix and sulphate and carbonate minerals.

Finally, these different approaches to mine dust indicated in this study demonstrate, as far as the study's researchers are aware, for the first time, the necessity of extracting the more deeply respirable size fraction of coal mine dusts in future studies on the health effects of such materials. This respirable fraction is geochemically different from the

parent materials, not only from the actual coal (and related sediments) being mined, but also from the coarser-grained passively-DDs found around the mine.

Authors statements

The corresponding author, Pedro Trechera, is responsible for ensuring that the descriptions are accurate and agreed by all authors, did the sampling and most of the analyses and most of writing.

Xavier Querol participated in the sampling and analysis, discussed results, also wrote some sections and reviewed the manuscript.

Zhuang Xinguo, Baoqing Li, Jing Li, Yunfei Shangguan and Patricia Córdoba, participated in the sampling of different mines, discussed results and reviewed the manuscript.

Ana Oliete and Frank Kelly did the OP analysis, wrote a section and reviewed the manuscript.

Teresa Moreno and Natalia Moreno performed SEM and DRX analyses, discussed results and reviewed the manuscript.

Declaration of Competing Interest

The authors declare that they have no known competing financial interests or personal relationships that could have appeared to influence the work reported in this paper.

Acknowledgements

This study was supported by Generalitat de Catalunya (AGAUR 2017 SGR41), Spain; by the National Science Foundation of China (grant 41972180); the Program of Introducing Talents of Discipline to Universities (grant B14031) and Overseas Top Scholars Program for the Recruitment of Global Experts, China and by the Spanish Ministry of Science and Innovation (Excelencia Severo Ochoa, Project CEX2018-000794-S). Pedro Trechera is contracted by the ROCD (Reducing risks from Occupational exposure to Coal Dust) project supported by the European Commission Research Fund for Coal and Steel; Grant Agreement Number-754205.

Appendix A. Supplementary data

Supplementary data to this article can be found online at https://doi.org/10.1016/j.coal.2021.103677.

References

Akinwekomi, V., Maree, J.P., Masindi, V., Zvinowanda, C., Osman, M.S., Foteinis, S., Mpenyana-Monyatsi, L., Chatzisymeon, E., 2020. Beneficiation of acid mine drainage (AMD): a viable option for the synthesis of goethite, hematite, magnetite, and gypsum – Gearing towards a circular economy concept. Miner. Eng. 148, 106204. https://doi.org/10.1016/J.MINENG.2020.106204.

Amato, F., Querol, X., Alastuey, A., Pandolfi, M., Moreno, T., Gracia, J., Rodriguez, P., 2009. Evaluating urban PM10 pollution benefit induced by street cleaning activities. Atmos. Environ. 43, 4472–4480. https://doi.org/10.1016/j.atmosenv.2009.06.037.

Amato, F., Querol, X., Johansson, C., Nagl, C., Alastuey, A., 2010. A review on the effectiveness of street sweeping, washing and dust suppressants as urban PM control methods. Sci. Total Environ. 408, 3070–3084. https://doi.org/10.1016/j.scitotenv.2010.04.025.

Azam, S., Mishra, D.P., 2019. Effects of particle size, dust concentration and dust-dispersion-air pressure on rock dust inertant requirement for coal dust explosion suppression in underground coal mines. Process. Saf. Environ. Prot. 126, 35–43. https://doi.org/10.1016/j.psep.2019.03.030.

Baker, M.A., Cerniglia, G.J., Zaman, A., 1990. Microtiter plate assay for the measurement of glutathione and glutathione disulfide in large numbers of biological samples. Anal. Biochem. 190, 360–365. https://doi.org/10.1016/0003-2697(90)90208-Q.

Birben, E., Sahiner, U.M., Sackesen, C., Erzurum, S., Kalayci, O., 2012. Oxidative stress and antioxidant defense. World Allergy Organ. J. 5, 9–19. https://doi.org/10.1097/WOX.0b013e3182439613.

Borm, P.J.A., 2002. Particle toxicology: from coal mining to nanotechnology. Inhal. Toxicol. 14, 311–324. https://doi.org/10.1080/08958370252809086.

BP (Ed.), 2019. 2019. BP Statistical Review of World Energy Statistical Review of World, pp. 1–69. Ed. BP Stat. Rev. World Energy.

Brodny, J., Tutak, M., 2018. Exposure to harmful dusts on fully powered longwall coal mines in Poland. Int. J. Environ. Res. Public Health 15. https://doi.org/10.3390/ijerph15091846.

Caballero-Gallardo, K., Olivero-Verbel, J., 2016. Mice housed on coal dust-contaminated sand: a model to evaluate the impacts of coal mining on health. Toxicol. Appl. Pharmacol. 294, 11–20. https://doi.org/10.1016/j.taap.2016.01.009.

Calas, A., Uzu, G., Kelly, F.J., Houdier, S., Martins, J.M.F., Thomas, F., Molton, F., Charron, A., Dunster, C., Oliete, A., Jacob, V., Besombes, J.-L., Chevrier, F., Jaffrezo, J.-L., 2018. Comparison between five acellular oxidative potential measurement assays performed with detailed chemistry on PM₁₀ samples from the city of Chamonix (France). Atmos. Chem. Phys. 18, 7863–7875. https://doi.org/10.5194/acp-18-7863-2018.

Casagrande, D.J., 1987. Sulphur in peat and coal. Geol. Soc. Spec. Publ. 32, 87–105. https://doi.org/10.1144/GSL.SP.1987.032.01.07.

Cassee, F.R., Mills, N.L., Newby, D. (Eds.), 2011. Cardiovascular Effects of Inhaled Ultrafine and Nanosized Particles, Cardiovascular Effects of Inhaled Ultrafine and Nanosized Particles. John Wiley & Sons, Inc., Hoboken, NJ, USA https://doi.org/10.1002/9780470910917.

Cassee, F.R., Morawska, L., Peters, A., 2019. Ambient Ultrafine Particles : Evidence for Policy Makers.

Castranova, V., 2000. From Coal Mine Dust to Quartz: Mechanisms of Pulmonary Pathogenicity. Inhal. Toxicol. 12, 7–14. https://doi.org/10.1080/08958378.2000.11463226.

Chen, F., Wang, S., Mou, S., Azimuddin, I., Zhang, D., Pan, X., Al-Misned, F.A., Mortuza, M.G., 2015. Physiological responses and accumulation of heavy metals and arsenic of Medicago sativa L. growing on acidic copper mine tailings in arid lands. J. Geochemical Explor. 157, 27–35. https://doi.org/10.1016/J.GEXPLO.2015.05.011.

Cheng, W., Yu, H., Zhou, G., Nie, W., 2016. The diffusion and pollution mechanisms of airborne dusts in fully-mechanized excavation face at mesoscopic scale based on CFD-DEM. Process. Saf. Environ. Prot. 104, 240–253. https://doi.org/10.1016/j.psep.2016.09.004.

Chung, F.H., 1974. Quantitative interpretation of X-ray diffraction patterns of mixtures. I. Matrix-flushing method for quantitative multicomponent analysis. J. Appl. Crystallogr. 7, 519–525. https://doi.org/10.1107/s0021889874010375.

Cohen, R.A.C., Patel, A., Green, F.H.Y., 2008. Lung disease caused by exposure to coal mine and silica dust. Semin. Respir. Crit. Care Med. https://doi.org/10.1055/s-0028-1101275.

Colinet, J.F., James, P.R., Jeffrey, M.L., John, A.O., Anita, L.W., 2010. Best Practices for Dust Control in Coal Mining. Centers Dis. Control Prev. Natl. Inst. Occup. Saf. Heal. 01, 17–36.

Dai, S., Finkelman, R.B., 2018. Coal as a promising source of critical elements: Progress and future prospects. Int. J. Coal Geol. 186, 155–164. https://doi.org/10.1016/j.coal.2017.06.005.

Dai, S.F., Zhou, Y.P., Ren, D.Y., Wang, X.B., Li, D., Zhao, L., 2007. Geochemistry and mineralogy of the late Permian coals from the Songzo Coalfield, Chongqing, southwestern China. Sci. China Ser. D Earth Sci. 50, 678–688. https://doi.org/10.1007/s11430-007-0001-4.

Dai, S., Ren, D., Zhou, Y., Chou, C.L., Wang, X., Zhao, L., Zhu, X., 2008. Mineralogy and geochemistry of a superhigh-organic-sulfur coal, Yanshan Coalfield, Yunnan, China: evidence for a volcanic ash component and influence by submarine exhalation. Chem. Geol. 255, 182–194. https://doi.org/10.1016/j.chemgeo.2008.06.030.

Dai, S., Li, T., Seredin, V.V., Ward, C.R., Hower, J.C., Zhou, Y., Zhang, M., Song, X., Song, W., Zhao, C., 2014. Origin of minerals and elements in the late Permian coals, tonsteins, and host rocks of the Xinde Mine, Xuanwei, eastern Yunnan, China. Int. J. Coal Geol. 121, 53–78. https://doi.org/10.1016/j.coal.2013.11.001.

Dai, S., Bechtel, A., Eble, C.F., Flores, R.M., French, D., Graham, I.T., Hood, M.M., Hower, J.C., Korasidis, V.A., Moore, T.A., Püttmann, W., Wei, Q., Zhao, L., O'Keefe, J.M.K., 2020. Recognition of peat depositional environments in coal: a review. Int. J. Coal Geol. https://doi.org/10.1016/j.coal.2019.103383.

Dalal, N.A.R.S., Newman, J., Pack, D., Leonard, S., Vallyathan, V.A.L., 1995. Original Contribution, 18, pp. 11–20.

Dias, C.L., Oliveira, M.L.S., Hower, J.C., Taffarel, S.R., Kautzmann, R.M., Silva, L.F.O., 2014. Nanominerals and ultrafine particles from coal fires from Santa Catarina, South Brazil. Int. J. Coal Geol. 122, 50–60. https://doi.org/10.1016/j.coal.2013.12.011.

Ercal, N.B.S.P., Hande Gurer-Orhan, B.S.P., Nukhet Aykin-Burns, B.S.P., 2005. Toxic Metals and Oxidative stress part I: mechanisms involved in Me-tal induced oxidative damage. Curr. Top. Med. Chem. 1, 529–539. https://doi.org/10.2174/1568026013394831.

Erol, I., Aydin, H., Didari, V., Ural, S., 2013. Pneumoconiosis and quartz content of respirable dusts in the coal mines in Zonguldak, Turkey. Int. J. Coal Geol. 116–117, 26–35. https://doi.org/10.1016/j.coal.2013.05.008.

Finkelman, R.B., 1994. Modes of occurrence of potentially hazardous elements in coal: levels of confidence. Fuel Process. Technol. 39, 21–34. https://doi.org/10.1016/0378-3820(94)90169-4.

Finkelman, R.B., Dai, S., French, D., 2019. The importance of minerals in coal as the hosts of chemical elements: a review. Int. J. Coal Geol. 212, 103251.

Fu, P.P., Xia, Q., Hwang, H.M., Ray, P.C., Yu, H., 2014. Mechanisms of nanotoxicity: generation of reactive oxygen species. J. Food Drug Anal. 22, 64–75. https://doi.org/10.1016/j.jfda.2014.01.005.

Gamble, F.J., 2012. Rapidly progressing coal workers pneumoconiosis as a confounding risk factor in assessing coal mine dust safe exposure levels. J. Clin. Toxicol. 01 https://doi.org/10.4172/2161-0495.s1-003.

Ghio, A.J., Madden, M.C., 2018. Human lung injury following exposure to humic substances and humic-like substances. Environ. Geochem. Health 40, 571–581. https://doi.org/10.1007/s10653-017-0008-5.

Giechaskiel, B., 2018. Solid particle number emission factors of euro vi heavy-duty vehicles on the road and in the laboratory. Int. J. Environ. Res. Public Health 15. https://doi.org/10.3390/ijerph15020304.

Gilmour, M.I., O'Connor, S., Dick, C.A.J., Miller, C.A., Linak, W.P., 2004. Differential pulmonary inflammation and in vitro cytotoxicity of size-fractionated fly ash particles from pulverized coal combustion. J. Air Waste Manage. Assoc. 54, 286–295. https://doi.org/10.1080/10473289.2004.10470906.

Gomo, M., 2018. Conceptual hydrogeochemical characteristics of a calcite and dolomite acid mine drainage neutralised circumneutral groundwater system. Water Sci. 32, 355–361. https://doi.org/10.1016/J.WSJ.2018.05.004.

Gürdal, G., 2008. Geochemistry of trace elements in Çan coal (Miocene), Çanakkale. Turkey. Int. J. Coal Geol. 74, 28–40. https://doi.org/10.1016/J.COAL.2007.09.004.

Heusinkveld, H.J., Wahle, T., Campbell, A., Westerink, R.H.S., Tran, L., Johnston, H., Stone, V., Cassee, F.R., Schins, R.P.F., 2016. Neurodegenerative and neurological disorders by small inhaled particles. Neurotoxicology 56, 94–106. https://doi.org/10.1016/j.neuro.2016.07.007.

Hower, J.C., Robertson, J.D., 2003. Clausthalite in coal. Int. J. Coal Geol. 53, 219–225. https://doi.org/10.1016/S0166-5162(03)00022-3.

Huang, X., Li, W., Attfield, M.D., Nádas, A., Frenkel, K., Finkelman, R.B., 2005. Mapping and prediction of coal Workers' Pneumoconiosis with bioavailable iron content in the bituminous coals. Environ. Health Perspect. 113, 964–968. https://doi.org/10.1289/ehp.7679.

Hung, N.T.Q., Lee, S.B., Hang, N.T., Kongpran, J., Kim Oanh, N.T., Shim, S.G., Bae, G.N., 2014. Characterization of black carbon at roadside sites and along vehicle roadways in the Bangkok Metropolitan Region. Atmos. Environ. 92, 231–239. https://doi.org/10.1016/j.atmosenv.2014.04.011.

Hussein, T., Saleh, S., dos Santos, V., Abdullah, H., Boor, B., 2019. Black carbon and particulate matter concentrations in eastern mediterranean urban conditions: an assessment based on integrated stationary and mobile observations. Atmosphere (Basel). 10, 323. https://doi.org/10.3390/atmos10060323.

IEA, 2019. World Energy Outlook 2019. IEA, Paris [WWW Document].

Iriyama, K., Yoshiura, M., Iwamoto, T., Ozaki, Y., 1984. Simultaneous determination of uric and ascorbic acids in human serum by reversed-phase high-performance liquid chromatography with electrochemical detection. Anal. Biochem. 141, 238–243. https://doi.org/10.1016/0003-2697(84)90451-2.

Johann-Essex, V., Keles, C., Rezaee, M., Scaggs-Witte, M., Sarver, E., 2017. Respirable coal mine dust characteristics in samples collected in central and northern Appalachia. Int. J. Coal Geol. 182, 85–93. https://doi.org/10.1016/j.coal.2017.09.010.

Kelly, F.J., 2003. Oxidative stress: its role in air pollution and adverse health effects. Occup. Environ. Med. 60, 612–616. https://doi.org/10.1136/oem.60.8.612.

Ketris, M.P., Yudovich, Y.E., 2009. Estimations of Clarkes for Carbonaceous biolithes: World averages for trace element contents in black shales and coals. Int. J. Coal Geol. 78, 135–148. https://doi.org/10.1016/j.coal.2009.01.002.

Kurth, L.M., McCawley, M., Hendryx, M., Lusk, S., 2014. Atmospheric particulate matter size distribution and concentration in West Virginia coal mining and non-mining areas. Mod. Pathol. 27, 405–411. https://doi.org/10.1038/jes.2014.2.

Latvala, S., Hedberg, J., Di Bucchianico, S., Möller, L., Wallinder, I.O., Elihn, K., Karlsson, H.L., 2016. Nickel release, ROS generation and toxicity of Ni and NiO micro- and nanoparticles. PLoS One 11, 1–20. https://doi.org/10.1371/journal.pone.0159684.

Lee, S., 1990. Oil Shale Technology, p. 280.

Li, N., Sioutas, C., Cho, A., Schmitz, D., Misra, C., Sempf, J., Wang, M., Oberley, T., Froines, J., Nel, A., 2003. Ultrafine particulate pollutants induce oxidative stress and mitochondrial damage. Environ. Health Perspect. 111, 455–460. https://doi.org/10.1289/ehp.6000.

Li, N., Xia, T., Nel, A.E., 2008. The role of oxidative stress in ambient particulate matter-induced lung diseases and its implications in the toxicity of engineered nanoparticles. Free Radic. Biol. Med. 44, 1689–1699. https://doi.org/10.1016/j.freeradbiomed.2008.01.028.

Li, J., Zhuang, X., Querol, X., Font, O., Moreno, N., Zhou, J., Lei, G., 2012. High quality of Jurassic Coals in the Southern and Eastern Junggar Coalfields, Xinjiang, NW China: Geochemical and mineralogical characteristics. Int. J. Coal Geol. 99, 1–15. https://doi.org/10.1016/j.coal.2012.05.003.

Liang, Y., Wong, O., Yang, L., Li, T., Su, Z., 2006. The development and regulation of occupational exposure limits in China. Regul. Toxicol. Pharmacol. 46, 107–113. https://doi.org/10.1016/j.yrtph.2006.02.007.

Liu, G., Vassilev, S.V., Gao, L., Zheng, L., Peng, Z., 2005. Mineral and chemical composition and some trace element contents in coals and coal ashes from Huaibei coal field, China. Energy Convers. Manag. https://doi.org/10.1016/j.enconman.2004.11.002.

Liu, Q., Bai, C., Li, X., Jiang, L., Dai, W., 2010. Coal dust/air explosions in a large-scale tube. Fuel 89, 329–335. https://doi.org/10.1016/j.fuel.2009.07.010.

Ma, D., Qin, B., Gao, Y., Jiang, J., Feng, B., 2020. Study on the explosion characteristics of methane–air with coal dust originating from low-temperature oxidation of coal. Fuel 260, 116304. https://doi.org/10.1016/j.fuel.2019.116304.

Madzivire, G., Petrik, L.F., Gitari, W.M., Ojumu, T.V., Balfour, G., 2010. Application of coal fly ash to circumneutral mine waters for the removal of sulphates as gypsum and ettringite. Miner. Eng. 23, 252–257. https://doi.org/10.1016/J.MINENG.2009.12.004.

Medeiros, M.A., Leite, C.M.M., Lago, R.M., 2012. Use of glycerol by-product of biodiesel to produce an efficient dust suppressant. Chem. Eng. J. 180, 364–369. https://doi.org/10.1016/j.cej.2011.11.056.

Morawska, L., Ristovski, Z., Jayaratne, E.R., Keogh, D.U., Ling, X., 2008. Ambient nano and ultrafine particles from motor vehicle emissions: Characteristics, ambient processing and implications on human exposure. Atmos. Environ. https://doi.org/10.1016/j.atmosenv.2008.07.050.

Moreno, T., Higueras, P., Jones, T., McDonald, I., Gibbons, W., 2005. Size fractionation in mercury-bearing airborne particles (HgPM 10) at Almadén, Spain: Implications for inhalation hazards around old mines. Atmos. Environ. 39, 6409–6419. https://doi.org/10.1016/j.atmosenv.2005.07.024.

Moreno, T., Kelly, F.J., Dunster, C., Oliete, A., Martins, V., Reche, C., Minguillón, M.C., Amato, F., Capdevila, M., de Miguel, E., Querol, X., 2017. Oxidative potential of subway PM2.5. Atmos. Environ. 148, 230–238. https://doi.org/10.1016/j.atmosenv.2016.10.045.

Moreno, T., Trechera, P., Querol, X., Lah, R., Johnson, D., Wrana, A., Williamson, B., 2019. Trace element fractionation between PM10 and PM2.5 in coal mine dust: Implications for occupational respiratory health. Int. J. Coal Geol. 203, 52–59. https://doi.org/10.1016/j.coal.2019.01.006.

Mudway, I.S., Stenfors, N., Duggan, S.T., Roxborough, H., Zielinski, H., Marklund, S.L., Blomberg, A., Frew, A.J., Sandström, T., Kelly, F.J., 2004. An in vitro and in vivo investigation of the effects of diesel exhaust on human airway lining fluid antioxidants. Arch. Biochem. Biophys. 423, 200–212. https://doi.org/10.1016/j.abb.2003.12.018.

Munir, M.A.M., Liu, G., Yousaf, B., Mian, M.M., Ali, M.U., Ahmed, R., Cheema, A.I., Naushad, M., 2020. Contrasting effects of biochar and hydrothermally treated coal gangue on leachability, bioavailability, speciation and accumulation of heavy metals by rapeseed in copper mine tailings. Ecotoxicol. Environ. Saf. 191, 110244. https://doi.org/10.1016/J.ECOENV.2020.110244.

NIOSH, 2002. Health effects of occupational exposure to respirable crystalline silica. NIOSH Hazard Rev. 145 doi:2002–129.

Oberdörster, G., Ferin, J., Lehnert, B.E., 1992. Correlation between particle size, in vivo particle persistence, and lung injury. Environ. Health Perspect. 102, 173–179. https://doi.org/10.1289/ehp.102-1567252.

Pedroso-Fidelis, G. Dos S., Farias, H.R., Mastella, G.A., Boufleur-Niekraszewicz, L.A., Dias, J.F., Alves, M.C., Silveira, P.C.L., Nesi, R.T., Carvalho, F., Zocche, J.J., Pinho, R.A., 2020. Pulmonary oxidative stress in wild bats exposed to coal dust: a model to evaluate the impact of coal mining on health. Ecotoxicol. Environ. Saf. 191, 110211. https://doi.org/10.1016/J.ECOENV.2020.110211.

Querol, X., Chinchon, S., Lopez-Soler, A., 1989. Iron sulfide precipitation sequence in Albian coals from the Maestrazgo Basin, southeastern Iberian Range, northeastern Spain. Int. J. Coal Geol. 11, 171–189. https://doi.org/10.1016/0166-5162(89)90004-9.

Querol, X., Fernandez Turiel, J.L., Lopez Soler, A., Duran, M.E., 1992. Trace elements in high-S subbituminous coals from the Teruel Mining District, Northeast Spain. Appl. Geochem. 7, 547–561. https://doi.org/10.1016/0883-2927(92)90070-J.

Querol, X., Whateley, M.K.G., Fernández-Turiel, J.L., Tuncali, E., 1997. Geological controls on the mineralogy and geochemistry of the Beypazari lignite, Central Anatolia, Turkey. Int. J. Coal Geol. 33, 255–271. https://doi.org/10.1016/S0166-5162(96)00044-4.

Querol, X., Alastuey, A., Rodriguez, S., Plana, F., Mantilla, E., Ruiz, C.R., 2001. Monitoring of PM10 and PM2.5 around primary particulate anthropogenic emission sources. Atmos. Environ. 35, 845–858. https://doi.org/10.1016/S1352-2310(00)00387-3.

Querol, X., Viana, M., Alastuey, A., Amato, F., Moreno, T., Castillo, S., Pey, J., de la Rosa, J., Sánchez de la Campa, A., Artíñano, B., Salvador, P., García Dos Santos, S., Fernández-Patier, R., Moreno-Grau, S., Negral, L., Minguillón, M.C., Monfort, E., Gil, J.I., Inza, A., Ortega, L.A., Santamaría, J.M., Zabalza, J., 2007. Source origin of trace elements in PM from regional background, urban and industrial sites of Spain. Atmos. Environ. 41, 7219–7231. https://doi.org/10.1016/J.ATMOSENV.2007.05.022.

Reche, C., Querol, X., Alastuey, A., Viana, M., Pey, J., Moreno, T., Rodríguez, S., González, Y., Fernández-Camacho, R., de la Rosa, J., Dall Osto, M., Prévôt, A.S.H., Hueglin, C., Harrison, R.M., Quincey, P., 2011. New considerations for PM, Black Carbon and particle number concentration for air quality monitoring across different European cities. Atmos. Chem. Phys. 11, 6207–6227. https://doi.org/10.5194/acp-11-6207-2011.

Richardson, C., Rutherford, S., Agranovski, I., 2018. Characterization of particulate emissions from Australian open-cut coal mines: toward improved emission estimates. J. Air Waste Manage. Assoc. 68, 598–607. https://doi.org/10.1080/10962247.2017.1415236.

Riley, K.W., French, D.H., Farrell, O.P., Wood, R.A., Huggins, F.E., 2012. Modes of occurrence of trace and minor elements in some Australian coals. Int. J. Coal Geol. 94, 214–224. https://doi.org/10.1016/j.coal.2011.06.011.

Rosita, W., Bendiyasa, I.M., Perdana, I., Anggara, F., 2020. Sequential particle-size and magnetic separation for enrichment of rare-earth elements and yttrium in Indonesia coal fly ash. J. Environ. Chem. Eng. 8, 103575. https://doi.org/10.1016/j.jece.2019.103575.

Sarver, E., Keles, C., Rezaee, M., 2019. Beyond conventional metrics: Comprehensive characterization of respirable coal mine dust. Int. J. Coal Geol. 207, 84–95. https://doi.org/10.1016/j.coal.2019.03.015.

Schins, R.P.F., Borm, P.J.A., 1999. Mechanisms and mediators in coal dust induced toxicity: a review. Ann. Occup. Hyg. 43, 7–33. https://doi.org/10.1016/S0003-4878(98)00069-6.

Sevim, Ö., Demir, İ., 2019. Optimization of fly ash particle size distribution for cementitious systems with high compactness. Constr. Build. Mater. 195, 104–114. https://doi.org/10.1016/j.conbuildmat.2018.11.080.

Shahan, M.R., Seaman, C.E., Beck, T.W., Colinet, J.F., Mischler, S.E., 2017. Characterization of airborne float coal dust emitted during continuous mining, longwall mining and belt transport. Min. Eng. 69, 61–66 doi:10.19150/me.7746.

Shi, G.Q., Han, C., Wang, Y. Ming, Wang, H.T., 2019. Experimental study on synergistic wetting of a coal dust with dust suppressant compounded with noncationic surfactants and its mechanism analysis. Powder Technol. 356, 1077–1086. https://doi.org/10.1016/j.powtec.2019.09.040.

Shimura, K., Matsuo, A., 2019. Using an extended CFD-DEM for the two-dimensional simulation of shock-induced layered coal-dust combustion in a narrow channel. Proc. Combust. Inst. 37, 3677–3684. https://doi.org/10.1016/j.proci.2018.07.066.

Soltani, N., Keshavarzi, B., Sorooshian, A., Moore, F., Dunster, C., Dominguez, A.O., Kelly, F.J., Dhakal, P., Ahmadi, M.R., Asadi, S., 2018. Oxidative potential (OP) and mineralogy of iron ore particulate matter at the Gol-E-Gohar Mining and Industrial Facility (Iran). Environ. Geochem. Health 40, 1785–1802. https://doi.org/10.1007/s10653-017-9926-5.

Sperazza, M., Moore, J.N., Hendrix, M.S., 2004. High-resolution particle size analysis of naturally occurring very fine-grained sediment through laser diffractometry. J. Sediment. Res. 74, 736–743. https://doi.org/10.1306/031104740736.

Suarthana, E., Laney, A.S., Storey, E., Hale, J.M., Attfield, M.D., 2011. Coal workers' pneumoconiosis in the United States: Regional differences 40 years after implementation of the 1969 Federal Coal Mine Health and Safety Act. Occup. Environ. Med. 68, 908–913. https://doi.org/10.1136/oem.2010.063594.

Trechera, P., Moreno, T., Córdoba, P., Moreno, N., Zhuang, X., Li, B., Li, J., Shangguan, Y., Kandler, K., Dominguez, A.O., Kelly, F., Querol, X., 2020. Mineralogy, geochemistry and toxicity of size-segregated respirable deposited dust in underground coal mines. J. Hazard. Mater. 399, 122935. https://doi.org/10.1016/j.jhazmat.2020.122935.

Valko, M., Jomova, K., Rhodes, C.J., Kuča, K., Musílek, K., 2016. Redox- and non-redox-metal-induced formation of free radicals and their role in human disease. Arch. Toxicol. https://doi.org/10.1007/s00204-015-1579-5.

WCA, 2020. World Coal Association [WWW Document]. URL. https://www.worldcoal.org/.

WHO, 2013. Review of Evidence on Health Aspects of Air Pollution – REVIHAAP Project Technical Report. World Health Organization. https://doi.org/10.1007/BF00379640.

Xi, Z., Jiang, M., Yang, J., Tu, X., 2014. Experimental study on advantages of foam–sol in coal dust control. Process. Saf. Environ. Prot. 92, 637–644. https://doi.org/10.1016/j.psep.2013.11.004.

Xu, C., Wang, D., Wang, H., Xin, H., Ma, L., Zhu, X., Zhang, Y., Wang, Q., 2017. Effects of chemical properties of coal dust on its wettability. Powder Technol. 318, 33–39. https://doi.org/10.1016/j.powtec.2017.05.028.

Yang, L., Zhu, Z., Li, D., Yan, X., Zhang, H., 2019. Effects of particle size on the flotation behavior of coal fly ash. Waste Manag. 85, 490–497. https://doi.org/10.1016/j.wasman.2019.01.017.

Zhang, X., Chen, W., Ma, C., Zhan, S., 2012. Modeling the effect of humidity on the threshold friction velocity of coal particles. Atmos. Environ. 56, 154–160. https://doi.org/10.1016/j.atmosenv.2012.04.015.

Zhao, C.L., Sun, Y.Z., Xiao, L., Qin, S.J., Wang, J.X., Duan, D.J., 2014. The occurrence of barium in a Jurassic coal in the Huangling 2 Mine, Ordos Basin, northern China. Fuel 128, 428–432. https://doi.org/10.1016/J.FUEL.2014.03.040.

Zhou, J., Zhuang, X., Alastuey, A., Querol, X., Li, J., 2010. Geochemistry and mineralogy of coal in the recently explored Zhundong large coal field in the Junggar basin, Xinjiang province, China. Int. J. Coal Geol. 82, 51–67. https://doi.org/10.1016/j.coal.2009.12.015.

Zielinski, H., Mudway, I.S., Bérubé, K.A., Murphy, S., Richards, R., Kelly, F.J., 1999. Modeling the interactions of particulates with epithelial lining fluid antioxidants. Am. J. Phys. Lung Cell. Mol. Phys. 277, 719–726. https://doi.org/10.1152/ajplung.1999.277.4.l719.